



# An efficient method for PET image denoising by combining multi-scale transform and non-local means

Abhishek Bal<sup>1</sup> · Minakshi Banerjee<sup>2</sup> · Rituparna Chaki<sup>1</sup> · Punit Sharma<sup>3</sup>

Received: 28 May 2019 / Revised: 14 February 2020 / Accepted: 13 April 2020 /

Published online: 8 August 2020

© Springer Science+Business Media, LLC, part of Springer Nature 2020

## Abstract

The diagnosis of dementia, particularly in the early stages is very much helpful with Positron emission tomography (PET) image processing. The most important challenges in PET image processing are noise removal and region of interests (ROIs) segmentation. Although denoising and segmentation are performed independently, but the performance of the denoising process significantly affects the performance of the segmentation process. Due to the low signals to noise ratio and low contrast, PET image denoising is a challenging task. Individual wavelet, curvelet and non-local means (NLM) based methods are not well suited to handle both isotropic (smooth details) and anisotropic (edges and curves) features due to its restricted abilities. To address these issues, the present work proposes an efficient denoising framework for reducing the noise level of brain PET images based on the combination of multi-scale transform (wavelet and curvelet) and tree clustering non-local means (TNLM). The main objective of the proposed method is to extract the isotropic features from a noisy smooth PET image using tree clustering based non-local means (TNLM). Then curvelet-based denoising is applied to the residual image to extract the anisotropic features such as edges and curves. Finally, the extracted anisotropic features are inserted back into the isotropic features to obtain an estimated denoised image. Simulated phantom and clinical PET datasets have been used in this proposed work for testing and measuring the performance in the medical applications, such as gray matter segmentation and precise tumor region identification without any interaction with other structural images like MRI or CT. The results in the experimental section show that the proposed denoising method has obtained better performance than existing wavelet, curvelet, wavelet-curvelet, non-local means (NLM) and deep learning methods based on the preservation of the edges. Qualitatively, a notable gain is achieved in the proposed denoised PET images in terms of contrast enhancement than other existing denoising methods.

---

✉ Abhishek Bal  
abhisheknew1991@gmail.com

<sup>1</sup> A.K. Choudhury School of Information Technology, University of Calcutta, Kolkata, India

<sup>2</sup> RCC Institute of Information Technology, Kolkata, India

<sup>3</sup> Apollo Gleneagles Hospital, Kolkata, India

**Keywords** PET · Denoising · Wavelet · Curvelet · Non-local means · Residual image

## 1 Introduction

Positron emission tomography (PET) technology is used in medical studies and several research purposes involved in living the organs like the brain. Identification of the brain volume of the PET image is the basic task of analyzing the functional images. The functional details are recorded through positron emission tomography (PET) technique that is very much helpful in the diagnosis of dementia in the early stage. It has the ability to identify the progressive loss of structure or function of neurons, including the death of neurons that play a very significant role in the early stages of dementia. Although the PET images play a significant role in early of dementia diagnosis and treatment evaluation, but there are several disadvantages too, i.e. the presence of reasonable noise, low spatial resolution, low contrast [39, 40], large variation in the shape and texture that make too much difficulties to process the PET images. These issues reduce the quality of the PET images.

Noise removal and region of interests (ROIs) segmentation are two most important parts of the PET image processing. Although denoising and segmentation [3, 4] can perform independently, but the outcomes of the denoising significantly affect the performance of the segmentation by preserving the small structural details. In order to reduce the noise level and better PET image quality, Gaussian filter was applied by several researchers to reconstruct the PET image [1, 22, 50]. Although, this filter achieves good performance for homogeneous regions, but it blurred the edges and reduces the spatial resolution of PET images. Several researchers have proposed wavelet [17, 25, 30, 33, 43–45, 49] and curvelet [12, 13, 41, 46] transforms based PET image denoising methods that improve the quality of PET image over Gaussian filter. Although the wavelet-only and curvlet-only based denoising methods perform better over Gaussian filter [51] but individually, these denoising methods are not well suited for handling both isotropic (smooth details) and anisotropic features (edges and curves) in PET images. Recently, non-local means (NLM) [21, 28] filtering have been proposed and applied to PET image denoising [52]. The advantage of the NLM is systemically applying all possible self-predictions throughout the image and similar local patches are used to determine the weight of a pixel. Although, NLM algorithm performs well for preserving the structural details, but their performance is reduced in the presence of high noise (low SNR) because the local patches that are used to determine the weight of the pixel, itself noisy. Recently, deep neural network based methods [18, 23] have been proposed PET image denoising. But in case of insufficient number of label images for training, the performance of the deep learning is reduced.

In order to overcome the weakness of individual wavelet, curvelet and NLM based denoising methods, an efficient PET image denoising framework has been proposed in this present work that combines the multi-scale transforms (wavelet and curvelet) and tree clustering based non-local means (TNLM) for enhancing contrast and edges in PET image. The block diagram of the proposed method is shown in Fig. 1a. The main objective of the proposed method is to extract the isotropic features from noisy smooth PET image using tree clustering based non-local means (TNLM). Then curvelet-based denoising is applied to the residual image to extract the anisotropic features such as edges and curves. Finally, an estimated denoised image is obtained after merging the extracted anisotropic features with the isotropic features. In this present work, tree clustering based non-local means (TNLM) method is implemented in order to reduce the computational time of the original non-local means (NLM). The basic objective of the presented TNLM is that patch comparison is

performed between the set of patches that have higher similarities, which is based on the preselection of patches. Here, preselection of the patches is done by the K-means based tree clustering. The details of the proposed method are described in Section 1.

The proposed method was tested on both simulated phantom and clinical PET datasets provided by Apollo Gleneagles Hospital, Kolkata, India for three types of noise such as Gaussian noise, Poisson noise and mixed Gaussian-Poisson noise with different noise levels. The performance of the proposed method has been compared with VisuShrink, BayesShrink, NeighShrink, ModiNeighShrink, curvelet, wavelet-curvelet, non-local means (NLM), vector non-local means and deep learning based methods. The visual and numerical results of the proposed method show that the present denoising method is able to reduce the noise level while preserving and enhancing the isotropic and anisotropic details as compared to the other existing methods. Qualitatively, the contrast was enhanced in proposed denoised PET image than other denoising methods. In order to show the usefulness of the proposed method, the proposed denoised images are used in medical applications such as precise tumor region identification and gray matter segmentation, which are shown in Section 4.6.

The rest of the paper is organized into four sections. Section 2 describes related work. The details of the proposed method along with few theoretical details are described in Section 3. Section 4 describes the experimental details. Finally, Section 5 presents the conclusion of the proposed work.

## 2 Related work

A wavelet-based universal thresholding technique called VisuShrink was proposed by Donoho et al. [19], where threshold kept fixed for all wavelet subbands. Chang et al. in Ref. [15] proposed a new soft adaptive wavelet coefficient thresholding technique called BayesShrink where the distinct threshold is used for different subbands and achieved better performances than universal threshold [19]. A review article was proposed in Ref. [44] for discussing the several wavelet-based PET image denoising techniques. The experimental results in Ref. [44] showed that wavelet based denoising methods preserved more image information compared to the Gaussian filter. In Ref. [11], Cai et al. incorporated the neighborhood characteristic to the VisuShrink method called NeighShrink [16] that improved the performance of denoising method over VisuShrink with respect to MSE, SNR, and PSNR. It is also experimentally observed that NeighShrink may produce blurred image due to suppression of too many details of wavelet coefficients. The problems of NeighShrink [16] was overcome in ModineighShrink [34] method. It is experimentally observed that ModineighShrink achieved better results than VisuShrink with respect to MSE, SNR, and PSNR. Another modification of NeighShrink was proposed by Om et al. [37] as considering the size of individual subband along with the neighborhood characteristic. The results of this method [37] achieved better performance over NeighShrink and ModineighShrink based on PSNR. A complete set of experiments on PET images based on several wavelet-based techniques [14, 20, 35, 48] were performed in Ref. [24]. In Ref. [46], a novel curvelet-based denoising method proposed by Starck et al. using the edge preservation properties of curvelet transform. This curvelet-based denoising method [46] has been widely applied [2, 29] on PET image and achieved better results than wavelet-based denoising techniques. For preserving the spatial resolution of the PET image, a combination of wavelet and curvelet transforms based denoising technique was proposed by Pogam et al. [29]. The experimental results of this method showed that the combination of wavelet and curvelet achieved better

results over wavelet-only, curvelet-only and Gaussian filtering based denoising techniques on the simulated and clinical PET database. In 2005, Buades et al. [9, 10] first introduced non-local means (NLM) based image denoising method which is based on the local averaging of all pixels in the image. They analyzed their method with different denoising methods by introducing a new measurement called method noise [9]. In Ref. [36], Nguyen et al. introduced non-local means (NLM) concept on PET image reconstruction by incorporating prior anatomical information. Although their proposed method performs well for identifying the ROIs with less percentage error, but this method will require the prior information from the anatomical image. In 2013, Dutta et al. [21] proposed an efficient denoising method for dynamic PET images based on the concept of non-local means (NLM). Dutta et al. made a few modifications on traditional NLM [9], such as spatiotemporal patches (used for finding the similarity) and the smoothing parameter based on the local information. In Ref. [42], Said et al. proposed a modified version of non-local means filter called Optimized Vector NLM (OVNLM). The proposed OVNLM reduces the computational complexity of the non-local means (NLM) by considering only those pixels which are most similar to each other. A probabilistic approach is used in their proposed method in order to find out the similarity. The experimental results of their method showed that it not only reduces the computational time over NLM but also achieved promising results. In Ref. [23], deep convolutional neural network (CNN) based denoising method has been proposed to pre-train the network on the simulated phantom data and then fine-tune the network using the real PET datasets. The network in Ref. [23] was pre-trained using the phantom datasets due to the limited number of clinical PET datasets. The results of this network achieved better performance over Gaussian and non-local means based denoising methods.

As observed from the study of the recent works, it is experimentally observed that the wavelet-based denoising methods improve the SNR value by filtering the noise in wavelet coefficients. Wavelet transform base denoising performs well for isotropic features, but this technique is not good enough for handling the anisotropic features (edges and curves). Because it removes the anisotropic features along with noise due to suppression of too many wavelet coefficients. Curvelet transforms based denoising [26, 46] solved the problem of wavelet denoising using the edge preservation property of curvelet transform. It achieved very promising results in anisotropic structured images [46], but this denoising method is not well suited for handling the isotropic structured image as compared to wavelet-based denoising [47]. These two transforms, therefore, exhibit complementary properties. Although, the denoising method proposed by Pogam et al. [29] proposed a combination of wavelet and curvelet which uses the thresholding of wavelet coefficients, but this method [29] is not good enough for handling both isotropic and anisotropic features. It removes important information along with noise due to the suppression of many wavelet coefficients during thresholding. On the other hand, this method [29] is computationally expensive as compared to other wavelet and curvelet based methods. Whereas non-local means based methods [9, 21, 42] reduce the noise level while preserving the structural details, but the performance of non-local means based methodss is reduced in the presence of high noise. It also reduces the contrast level of an image. Beside of these, non-local means takes large computational time as compared to wavelet and curvelet based methods due to the too many weights calculation. Although the vector based non-local means reduces the computational time over the non-local means referred in Ref. [9], but still this method is not suitable for handling the anisotropic features in the presence of high Poisson and mixed Gaussian-Poisson noise. Whereas deep neural networks (DNNs) have been successfully applied in various image processing applications such as PET image denoising, but the performance of the deep learning [23] based method is dropped when the lack of a sufficient number of

training images. In order to handle such issues, some authors trained their network using the MRI/CT or simulated phantom datasets and then fine-tuned [23] using the real PET datasets. In essence, this implies that prior knowledge is used as network input to perform PET denoising. Beside of these, deep learning based denoising methods require larger computational time as compared to other methods. In order to handle these issues, the present work proposes an effective contrast and edge preservation based PET image denoising technique that integrates multi-scale transform (wavelet and curvelet) and tree clustering based non-local means (TNLM) to handle the weakness of wavelet-only, curvelet-only and NLM based methods. The proposed work does not utilize any anatomical knowledge of the structural images such as MRI and CT during the PET image denoising. A tree clustering based non-local means also presented on the behalf of traditional non-local means in order to reduce the computational time of non-local means. The main objective of the proposed work is to implement an efficient PET image denoising technique that can handle both isotropic and anisotropic features and helps in the case of medical applications such as gray matter segmentation and precise tumor region identification.

### 3 Materials and methods

#### 3.1 Proposed denoising framework

The block diagram of the proposed method is shown in Fig. 1a. The outcome of each step of the proposed denoising model (Fig. 1a) is shown in Fig. 1b. The four modules of the proposed method are as follows:

- **Module 1:** 2D wavelet decomposition to noisy PET image ( $I$ ) and extract the smooth details (approximate subband)  $I_A$ .
- **Module 2:** Tree clustering based non-local means (TNLM) is applied to smooth details ( $I_A$ ) and produces isotropic features (smooth denoised image)  $I_{ANLM}$ .
- **Module 3:** Compute the residual image ( $R$ ) which contains noise and anisotropic features.

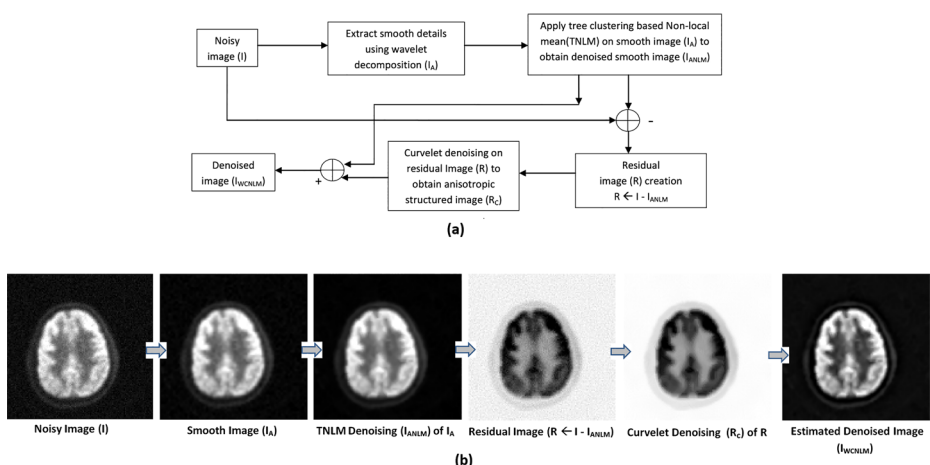


**Fig. 1** Block diagram of proposed denoising model. a Several steps of the proposed method, b corresponding outputs

- **Module 4:** Apply curvelet denoising to the residual image ( $R$ ) using the edge preservation property of curvelet [46] and extract the anisotropic information ( $R_C$ ), which are finally inserted back into the smooth denoised image ( $I_{ANLM}$ ) to obtain a final estimated denoised image ( $I_{WCNLM}$ ).

Each of the four modules is described in following sub-sections.

### 3.1.1 Module 1: Smooth details extraction

Initially, 2D wavelet transformation is applied to noisy PET image  $I$   $\{I_{i,j}$ , where  $i, j = 1, 2, \dots, N\}$  to obtain first level subbands namely approximate subband ( $LL_1$ ) and details subband ( $LH_1$ ,  $HL_1$  and  $HH_1$ ). Then we remove the details subband ( $LH_1$ ,  $HL_1$  and  $HH_1$ ) by initializing 0 (zero) and apply inverse 2D wavelet transform. The resulted image holds only smooth details ( $I_A$ ) of the original image ( $I$ ) whose size is same as original image size, which is shown in the second image of Fig. 1b. First level 2D wavelet transform is shown in Fig. 2.

### 3.1.2 Module 2: Tree clustering based NLM on smooth image details

Non-local means (NLM) filtering computes weighted average of the pixel intensities by assigning the large weight to the pixels which are more similar to the target pixel in terms of their local neighborhoods or patches. The NLM first introduced by Buades et al. [9, 10] for image denoising. The details about non-local means are described in Refs. [9, 10]. In the NLM, most of the computational time is spent on computing the distance between patches throughout the image. But the reality is that only a fraction of similar patches are well enough to compute the weight. To speed up the denoising process, different researches have been proposed depending on the preselection [8, 31, 38] of patches. Few of them are based on the similarity of patches mean [31] and standard deviation. Although these strategies significantly improve the speed of the denoising process, but the problem is that, two patches with same mean and standard deviation does not signify that they are similar in terms of neighborhood point of view.

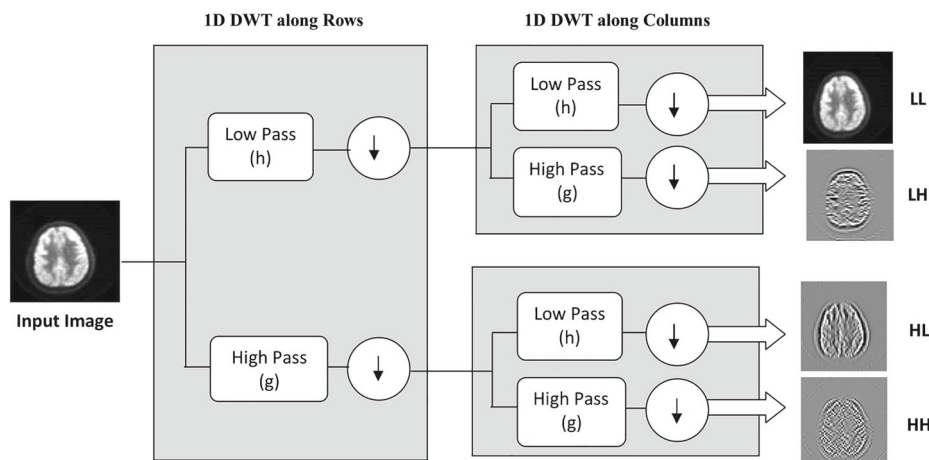


**Fig. 2** Block diagram of first level wavelet decomposition

In order to handle the above issue, the present work implements an efficient non-local means algorithm that incorporates K-means based tree clustering for preselecting the patches to improve the speed and the quality of the denoised image. The steps of tree clustering based NLM (TNLM) on the smooth image ( $I_A$ ) are as follows:

- Initially,  $5 \times 5$  patch for each pixel is extracted from the smooth image ( $I_A$ ). For example, in Fig. 3a, light gray area is considered as original image. In order to extract the patches, zero padding is done surrounding of the image, which is denoted by dark gray color in Fig. 3a. Then, for each pixel in light gray portion,  $5 \times 5$  patch is extracted, which is shown in Fig. 3b. Here,  $5 \times 5$  window is used for patch selection, which moves from left to right by shifting one position each time.
  - Apply hard clustering (K-means) on the root node (collection of all patches) (Fig. 4) with two clusters that splits the patches into two distinct clusters (child nodes). Each cluster (child node) contains similar patches. For example, patch containing the central pixel  $a_{34}$  (see Fig. 3b) goes one of the two clusters (nodes). These two distinct clusters denote the nodes of the first level of the binary tree (Fig. 4).
  - Again, each node (collection of distinct patches) of the first level is decomposed into two distinct clusters (nodes). This decomposition process is continued recursively until each leaf node contains approximately  $N_{thre} = 25$  number of patches. It is experimentally observed that approximate 25 number of similar patches are enough for performing the similarity measurement of a pixel using its neighborhood (patch).
  - The total number of K-means clustering is required for decomposition is at most  $2^{h-1}-1$ , where  $h$  is the height of the binary tree. Here, at most  $2^{h-1}-1$  times K-means is required instead of  $2^h-1$  (total number of nodes with height  $h$ ) because K-means is applied to each internal node. We highlight the term “at most” because the last level in this binary tree may not have maximum number of nodes or all the leaf nodes may not belong to the same level. This decomposition does not take much time because the K-means algorithm requires linear times in nature.

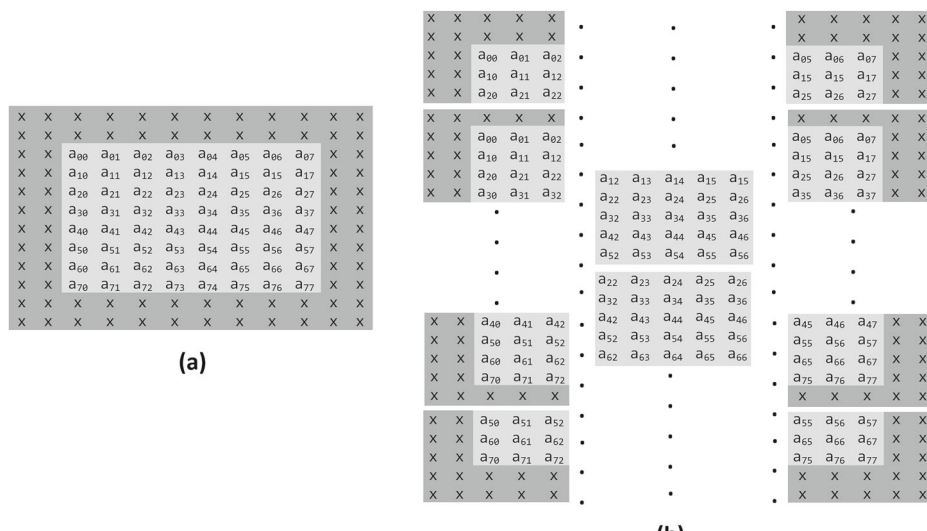


**Fig. 3** Patch creation for tree clustering based NLM. **a** Original image (light gray color) with zero padding (black border). **b** Extracted patches

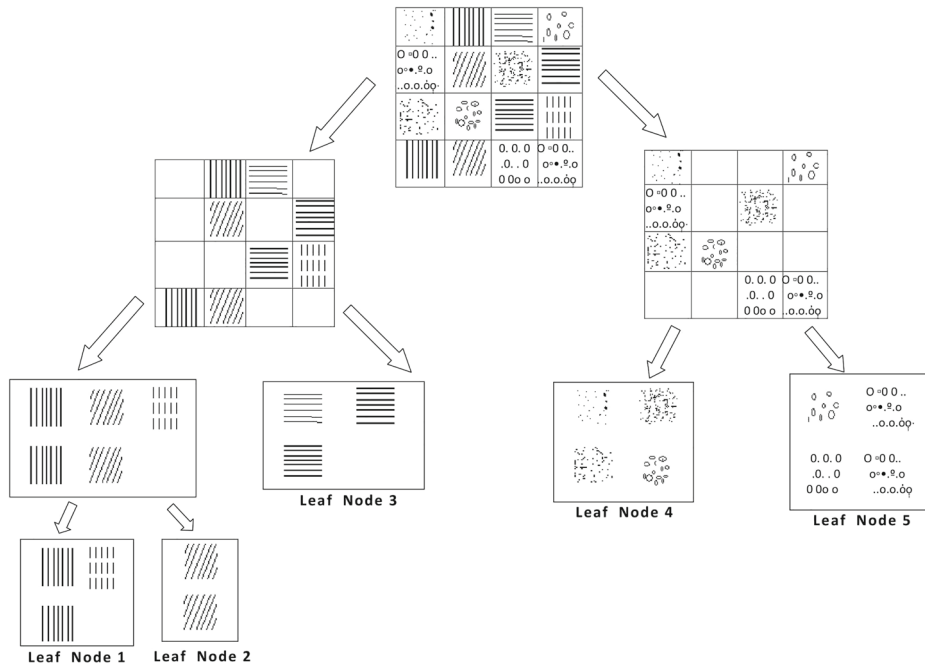


**Fig. 4** Pictorial illustration of a cluster tree. The leaf nodes contain a relatively small set of similar patches

- After decomposition, each leaf node from left to right is assigned by a distinct cluster number  $i$  ( $i = 1, 2, 3, \dots, n$ ), where  $n$  is the number of leaf nodes. An index matrix is created to maintain the leaf node number for each patch.
- Once the cluster tree has been built up, non-local-means (NLM[V(i)]) algorithm is applied to each  $i^{th}$  pixel of the smooth image ( $I_A$ ). To find the weighted average of the  $i^{th}$  pixel, the proposed method considers the patch (neighborhood window) surrounding of the  $i^{th}$  pixel, then check in which leaf node this patch belongs to, using the index matrix. After getting the leaf node number, only the patches that belong to that leaf node (collection of distinct patches) are considered as the similar patches and participate in the weighted average computation using the (1).  $NL[V(i)]$  [9] in (1) denotes the estimated value of  $i^{th}$  pixel after NLM.

$$NL[V(i)] = \sum_{\substack{j \in LN \\ LN(i) == LN(j)}} W(i, j) V(j) \quad (1)$$

where  $\{W(i, j)\}_i$  is the family of weights, which is based on the similarity between  $i^{th}$  and  $j^{th}$  pixels. Here,  $j^{th}$  pixel's patch must belong to the leaf node where the  $i^{th}$  pixel's patch is belong to. In (1),  $LN(i)$  and  $LN(j)$  denote the leaf nodes, which contain the patch of  $i^{th}$  pixel and  $j^{th}$  pixel respectively. The patch (neighborhood window) of  $i^{th}$  and  $j^{th}$  pixel are represented by  $N_i$  and  $N_j$  respectively, and the weight function ( $W(i, j)$ ) [9] is represented as:

$$W(i, j) = \frac{1}{Z(i)} e^{\frac{-\|V(N_i) - V(N_j)\|_{2,a}^2}{h^2}} \quad (2)$$

where  $h$  is the filter parameter that depends on the standard deviation of noise.  $Z(i)$  [9] is the normalized constant, which is defined as:

$$Z(i) = \sum_j e^{-\frac{\|V(N_i) - V(N_j)\|_{2,a}^2}{h^2}} \quad (3)$$

The similarity between two pixels in  $i^{th}$  and  $j^{th}$  positions are measured by weighted Euclidean distance  $\|V(N_i) - V(N_j)\|_{2,a}^2$ , where  $a (> 0)$  is used as the standard deviation of the Gaussian kernel. The weight function ( $W(i, j)$ ) [9] must satisfy the following two conditions:

$$0 \leq W(i, j) \leq 1 \quad (4)$$

$$\sum_j W(i, j) = 1 \quad (5)$$

In this TNLM,  $5 \times 5$  patches are considered and the value of the smoothing parameter ( $h$ ) is set to  $h^2 = 2\sigma^2$ . During weight computation, a small set of similar patches can be accessed from the leaf node in constant time using the index matrix. Note that, sometimes it may happen that one patch may have a similar probability to belong to more than one cluster. But due to hard clustering, this situation is ignored here and it is considered that each patch (neighborhood window) belongs to one of the distinct clusters.

Presented TNLM not only reduces the computational load, but also improves the quality of the denoised PET image by selecting similar patches in advance using the K-means based tree clustering.

Using the above tree clustering based non-local means (TNLM), the isotropic features or smooth details ( $I_{ANLM}$ ) are extracted from the noisy smooth image ( $I_A$ ). Next, the anisotropic features like the edges and curves of the noisy PET image are extracted using the curvelet-based denoising which is described next.

### 3.1.3 Module 3: Construction of residual image

To recover the anisotropic features (edges and curves), the residual image ( $R$ ) is calculated by subtracting the smooth denoised image ( $I_{ANLM}$ ) from the original noisy image ( $I$ ). The residual image ( $R$ ) [5] contains noise as well as edge information (anisotropic features), shown in (6).

$$R = I - I_{ANLM} \quad (6)$$

Alternatively, the residual image ( $R$ ) has been defined to be a function of anisotropic features (edges or curve) ( $I_{ANI}$ ) and noise ( $I_N$ ), which is represented as

$$R = I_{ANI} + I_N \quad (7)$$

During TNLM, the anisotropic features ( $I_{ANI}$ ) like edges or sharp boundaries are not filtered. So, the next essential step is to estimate those features from residual image ( $R$ ) using curvelet.

### 3.1.4 Module 4: Curvelet denoising based anisotropic features extraction

In order to extract the anisotropic features from the residual image ( $R$ ), curvelet transformation ( $\gamma_\mu$ ) based denoising is applied to the residual image ( $R$ ) using the edge preservation property of curvelet. According to the method described in Ref. [46], “à tours” filtering

algorithm is well adapted for the curvelet decomposition into several subbands. In this present work, we decompose the residual image ( $R$ ) [5, 46] using the following equation:

$$R(p, q) = \sum_{j=1}^J D_j(p, q) + S_J(p, q). \quad (8)$$

where  $S_J$  and  $D_j$  refer the smooth details of residual image ( $R$ ) and the detail subbands at scale  $2^{-j}$  respectively. Due to the non-preserving nature of curvelet transform, Starck et al. [46] finds the variance of noisy curvelet coefficients based on the curvelet index  $\lambda$ . For that reason, to denoise the curvelet coefficients,  $\sigma_\lambda^2$  of the individual variances is calculated in this present work with the presence of Monte-Carlo simulation. The following equation is used to threshold the noisy curvelet coefficients ( $y_\lambda$ ).

$$\widehat{y}_\lambda = \begin{cases} y_\lambda & \text{if } |y_\lambda|/\sigma \geq k\sigma_\lambda \\ 0 & \text{if } |y_\lambda|/\sigma < k\sigma_\lambda. \end{cases} \quad (9)$$

where  $\sigma$  is the noise standard deviation. In above (9), the value of  $k$  [46] is scale dependent. If  $j = 1, k = 4$  otherwise  $k = 3$ . The details about the image denoising using curvelet transform is described in Ref. [46]. Finally curvelet based denoised image ( $I_{ANI}$ ) (anisotropic features) is obtained after applying the inverse curvelet transform to the thresholded curvelet coefficients. These extracted features ( $I_{ANI}$ ) are merged with the smooth denoised image ( $I_{ANLM}$ ) to achieve an estimated denoised image ( $I_{WCND}$ ) using the following equation:

$$I_{WCND} = I_{ANLM} + I_{ANI}. \quad (10)$$

### 3.2 Algorithm

The proposed PET image denoising algorithms are as follows:

---

**Algorithm 1** Proposed denoising using multi-scale transform and tree clustering based non-local means (TNLM).

---

**Procedure:**  $WCTCNLM_{denoising}(\mathcal{I}, \mathcal{L}, \mathcal{W}_{type}, \mathcal{C}_{type})$

INPUT:

- Noisy image,  $\mathcal{I}$
- Wavelet decomposition level,  $\mathcal{L}$
- Wavelet type,  $\mathcal{W}_{type}$
- filtering parameter,  $\mathcal{F}_h$
- tree type parameter,  $\mathcal{C}_{type}$

OUTPUT:

- Estimated noiseless image,  $\mathcal{I}_{WCND}$

Steps:

- 1:  $[\mathcal{A}, \mathcal{H}, \mathcal{V}, \mathcal{D}] \leftarrow \psi(\mathcal{I}, \mathcal{L}, \mathcal{W}_{type}) \triangleright$  first level wavelet decomposition.
  - 2:  $\mathcal{H}' \leftarrow \mathcal{V}' \leftarrow \mathcal{D}' \leftarrow \mathcal{ZEROS}(\mathcal{S}\mathcal{L}\mathcal{Z}\mathcal{E}(\mathcal{I}))/2 \triangleright$  details subband initialization by 0.
  - 3:  $\mathcal{I}_A \leftarrow \psi^{-1}(\mathcal{A}, \mathcal{H}', \mathcal{V}', \mathcal{D}') \triangleright$  smooth noisy image creation.
  - 4:  $\mathcal{I}_{ANLM} \leftarrow \mathcal{T}\mathcal{C}\mathcal{N}\mathcal{L}\mathcal{M}(\mathcal{I}_A, \mathcal{F}_h, \mathcal{C}_{type}) \triangleright$  tree clustering based NLM.
  - 5:  $\mathcal{R} \leftarrow \mathcal{S}_{SUB}(\mathcal{I}, \mathcal{I}_{ANLM}) \triangleright$  residual image creation.
  - 6:  $\mathcal{I}_{ANI} \leftarrow \gamma(\mathcal{R}) \triangleright$  curvelet denoising on residual image.
  - 7:  $\mathcal{I}_{WCND} \leftarrow \mathcal{A}_{ADD}(\mathcal{I}_{ANLM}, \mathcal{I}_{ANI}) \triangleright$  merging of isotropic and anisotropic features.
  - 8: **return**  $\mathcal{I}_{WCND}$
-

**Algorithm 2** Tree clustering based NLM denoising**Procedure:** TCNLM( $\mathcal{I}_A, \mathcal{NW}, \mathcal{SW}, \mathcal{F}_h, \mathcal{C}_{type}$ )

INPUT:

- smooth image,  $\mathcal{I}_A$
- neighborhood window,  $\mathcal{NW}$
- search window,  $\mathcal{SW}$
- filtering parameter,  $\mathcal{F}_h$
- tree type parameter,  $\mathcal{C}_{type}$

OUTPUT:

- Estimated smooth denoised image,  $\mathcal{I}_{ANLM}$

**Steps:**

- 1:  $\mathcal{FV} \leftarrow \mathcal{NEIEXTRAC}(\mathcal{I}_{APPX}, \mathcal{NW})$   $\triangleright$  patches creation.
- 2:  $\mathcal{LN} \leftarrow \mathcal{TREECCLUSTER}(\mathcal{FV}, \mathcal{C}_{type})$   $\triangleright$  cluster tree creation.
- 3: **for all**  $i \in \mathcal{I}_A$  **do**
- 4:    $S_{weight} \leftarrow 0$   $\triangleright$  weight initialization for pixel  $i$ .
- 5:    $\mathcal{AVG} \leftarrow 0$
- 6:   **for all**  $j \in \mathcal{LN}$  **AND**  $\mathcal{LN}_i == \mathcal{LN}_j$  **do**  $\triangleright$  all patches that belong to the node where  $i^{th}$  pixel's patch belongs.
- 7:      $\mathcal{W}_{ij} \leftarrow \varphi(\mathcal{NW}_i, \mathcal{NW}_j, \mathcal{F}_h)$   $\triangleright$  weight calculation between patches of  $i^{th}$  and  $j^{th}$  pixels.
- 8:      $S_{weight} \leftarrow S_{weight} + \mathcal{W}_{ij}$
- 9:      $\mathcal{AVG} \leftarrow \mathcal{AVG} + \mathcal{W}_{ij} \times \mathcal{I}_{APPX}(j)$
- 10:   **end for**
- 11:    $\mathcal{I}_{ANLM}(i) \leftarrow \mathcal{AVG} / S_{weight}$   $\triangleright$  denoised smooth image.
- 12: **end for**
- 13: **return**  $\mathcal{I}_{ANLM}$

### 3.3 Data

A small description of the simulated phantom and clinical PET datasets [5] are described below.

#### 3.3.1 Simulated phantom datasets

All the digital synthetic brain PET reference images are downloaded from <http://depts.washington.edu/petcdro>. The digital PET reference for the brain  $^{18}\text{F}$ -FDG ( $^{18}\text{F}$ -Fludeoxyglucose) is a set of synthetically generated DICOM files with knowing the voxel information. These PET images were generated by segmenting human brain MR images, then artificially assigning PET standardized uptake value (SUV) with 1.67:1 (white matter: gray matter). The size of the 3D PET image is  $256 \times 256 \times 256$  with voxel size  $1 \times 1 \times 1 \text{ mm}^3$ .

#### 3.3.2 Clinical datasets

Clinical PET datasets provided by Apollo Gleneagles Hospital, Kolkata, India. These clinical PET images are constructed by Ingenuity TF PET/CT system with Astonish 3rd generation

time-of-flight (TOF) technology manufactured by Philips Company. The Ingenuity TF PET/CT combines the performance of Philips Astonish TF Time-of-Flight PET technology with CT advances like Philips iPatient, iDose<sup>4</sup> and metal artifact reduction for implants (O-MAR). In our proposed method 100 patients' clinical PET datasets (90 slices in each patient) are considered. The dimension of each patient PET brain is  $128 \times 128 \times 90$ . All the images are in DICOM format with 16-bit gray level. More information about this PET scanning is available at <http://www.philips.co.in/healthcare/product/HC882456/>.

### 3.4 Quantitative analysis

The quantitative metrics for evaluation of the proposed denoising method and other methods are briefly described in this section. The brief details of the quantitative metrics are as follows:

**Peak Signal-to-Noise Ratio (PSNR)** PSNR is represented as a ratio between maximum power generated by signal and the power of corrupting noise. The quality of the estimated denoised image is measured by PSNR and represented in terms of logarithmic decibel scale (11).

$$PSNR = 10 \times \log_{10} \frac{(2^n - 1)^2}{MSE} \quad (11)$$

$$MSE = \frac{\sum_{m=0}^{N-1} \sum_{n=0}^{N-1} [X(m, n) - \widehat{X}(m, n)]^2}{N \times N}. \quad (12)$$

where  $n$  represents the number of bits for representing the image. Generally, the better performance of the denoising method is denoted by the higher value of PSNR. In (11),  $X$  is the noise free image and  $\widehat{X}$  is the estimation of  $X$  after applying the denoising method.

**Contrast:** The contrast is used to measure the difference in luminance that distinguishes an object from others. The present work considers the local contrast [7] for measuring the performance of the proposed method. The local contrast  $C_{mn}$  of pixel position  $(m, n)$  has been defined to be a function of gray scale value ( $I_{mn}$ ) and mean gray level ( $\overline{E}_{mn}$ ) of the points that located at the boundaries of the object.  $\overline{E}_{mn}$  is defined as:

$$\overline{E}_{mn} = \frac{\sum_{i,j \in B_{mn}} \Delta_{ij} I_{ij}}{\sum_{i,j \in B_{mn}} \Delta_{ij}} \quad (13)$$

where  $B_{mn}$  is the neighborhood window of the pixel  $(m, n)$ . In our measurement, we choose  $3 \times 3$  window ( $B_{mn}$ ).  $\Delta_{ij}$  denotes the edge value of pixel  $(i, j)$  that resides within the window  $B_{mn}$ . The local contrast ( $C_{mn}$ ) [7] is formulated as:

$$C_{mn} = \frac{|I_{mn} - \overline{E}_{mn}|}{|I_{mn} + \overline{E}_{mn}|} \quad (14)$$

The contrast in the PET image plays a vital role in the visual interpretation of the image and it has a significant contribution during the segmentation.

**Edge value:** Edge value represents how each point of an image should contribute to the segmentation method. The rate of changes of gray level at a point is determined by edge value. As per as the Ref. [32], the edge value of the point  $I_{m,n}$  is formulated as:

$$\begin{aligned} E_{m,n} = \frac{1}{4} \max \{ & |I_{m-1,n} + I_{m-1,n+1} + I_{m,n} + I_{m,n+1} - I_{m+1,n} - I_{m+1,n+1} - I_{m+2,n} \\ & - I_{m+2,n+1}|, |I_{m,n-1} + I_{m,n} + I_{m+1,n-1} + I_{m+1,n} - I_{m,n+1} - I_{m,n+2} \\ & - I_{m+1,n+1} - I_{m+1,n+2}| \} \end{aligned} \quad (15)$$

Generally, a point inside of an object should have lower edge values, whereas a point on the border of an object should have higher edge value.

## 4 Experimental results

This section shows the denoising performance of the different methods (VisuShrink [19], BayesShrink [15], NeighShrink [16], ModineighShrink [34], ModineighShrink [37], Curvelet [46], Wavelet-Curvelet [29], Non-local means (NLM) [9], Vector Non-local means [42], and Deep learning [23]) along with the proposed method. The MATLAB 8.6 is used for implementing the proposed denoising method.

During the acquisition process, clinical PET data are corrupted with different noise levels. In order to handle such problem, initially simulated phantom is taken, then corrupt the image by adding or applying some known noise. Alternatively, the clinical PET image can be considered as a noise-free image, then some known noise like Gaussian noise or Poisson noise or mixed Gaussian-Poisson noise is added or applied with different levels to corrupt it. For extensive experimentation, both simulated phantom PET and clinical F-FDG (F-Fludeoxyglucose) PET images have been corrupted manually with different noise levels. The experimental results of the proposed method along with other denoising methods on the simulated phantom and clinical PET datasets are shown in bellow:

### 4.1 Results on simulated phantom datasets

The experimental results of different noise removal techniques along with the proposed method are reported in this section for three different types of noise such as Gaussian, Poisson and mixed Gaussian-Poisson noise. Figures 5, 6, 7 and 8 show original simulated PET phantom, noisy version (Gaussian, Poisson and mixed Gaussian-Poisson) of phantom and denoised images as obtained by different denoising methods. Tables 1, 2, 3 and 4 depict the PSNR, contrast and edge value obtained by different denoising algorithms, including proposed algorithm with  $5 \times 5$  patch. In Table 1, comparative performance analysis of different denoising algorithms is reported after applying the Gaussian noise on simulated PET (Fig. 5b) with respect to PSNR, contrast and edge value. Whereas Table 2 shows the performance of the same algorithms after applying the Poisson noise on simulated PET (Fig. 6b) image. The performance of the proposed method is also measured for mixed Gaussian-Poisson noise on simulated PET image (Figs. 7b and 8b) with respect to PSNR, contrast and edge value which is reported in Tables 3 and 4. The results in Tables 1, 2, 3 and 4 show that the proposed method achieves better results than other existing methods on simulated phantom brain PET reference images for three types of noise such as Gaussian, Poisson and mixed Gaussian-Poisson noise based on contrast and edge value.

**Fig. 5** Performance comparison of various denoising techniques for Gaussian noise on clinical brain PET with PSNR = 23 dB. **a** Original, **b** noisy image, **c** VisuShrink [19], **d** BayesShrink [15], **e** NeighShrink [16], **f** ModineighShrink [34], **g** ModineighShrink [37], **h** Curvelet [46], **i** Wavelet curvelet [29], **j** Non-local means (NLM) [9], **k** Vector Non-local means [42], **l** Deep learning [23], **m** proposed wavelet curvelet NLM (WCNLM)

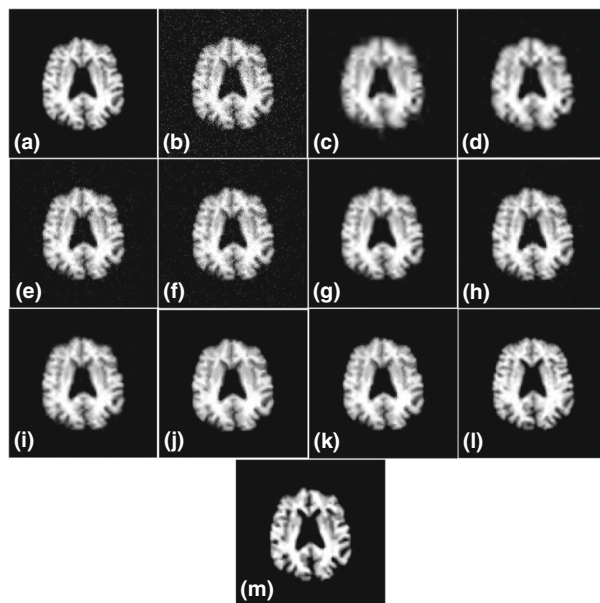


**Fig. 6** Performance comparison of various denoising techniques for Poisson noise ( $1e15$ ) on clinical brain PET with PSNR = 26 dB. **a** Original, **b** noisy image, **c** VisuShrink [19], **d** BayesShrink [15], **e** NeighShrink [16], **f** ModineighShrink [34], **g** ModineighShrink [37], **h** Curvelet [46], **i** Wavelet curvelet [29], **j** Non-local means (NLM) [9], **k** Vector Non-local means [42], **l** Deep learning [23], **m** proposed wavelet curvelet NLM (WCNLM)

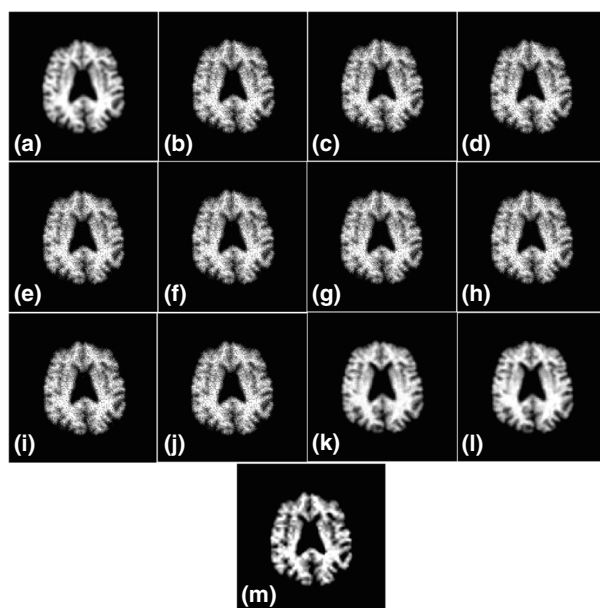


**Fig. 7** Performance comparison of various denoising techniques for mixed Gaussian-Poisson noise ( $1e15$ ) on simulated PET with PSNR = 20 dB. **a** Original, **b** noisy image, **c** VisuShrink [19], **d** BayesShrink [15], **e** NeighShrink [16], **f** ModineighShrink [34], **g** ModineighShrink [37], **h** Curvelet [46], **i** Wavelet curvelet [29], **j** Non-local means (NLM) [9], **k** Vector Non-local means [42], **l** Deep learning [23], **m** proposed wavelet curvelet NLM (WCNLM)

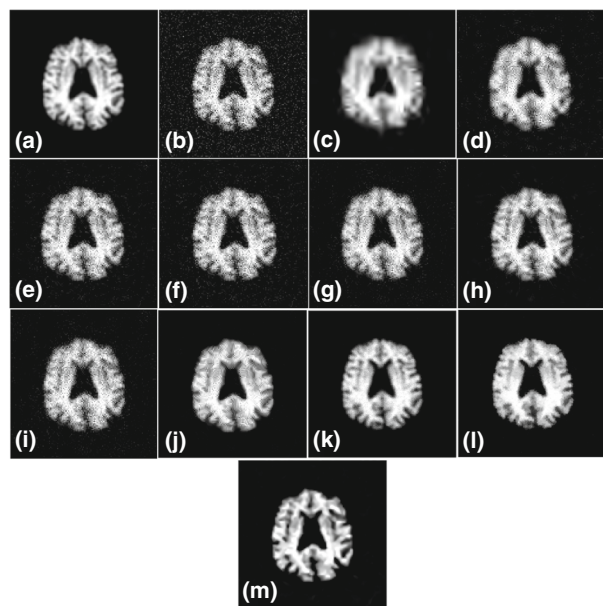


**Fig. 8** Performance comparison of various denoising techniques for mixed Gaussian-Poisson noise ( $1e14$ ) on simulated PET with PSNR = 20 dB. **a** Original, **b** noisy image, **c** VisuShrink [19], **d** BayesShrink [15], **e** NeighShrink [16], **f** ModineighShrink [34], **g** ModineighShrink [37], **h** Curvelet [46], **i** Wavelet curvelet [29], **j** Non-local means (NLM) [9], **k** Vector Non-local means [42], **l** Deep learning [23], **m** proposed wavelet curvelet NLM (WCNLM)

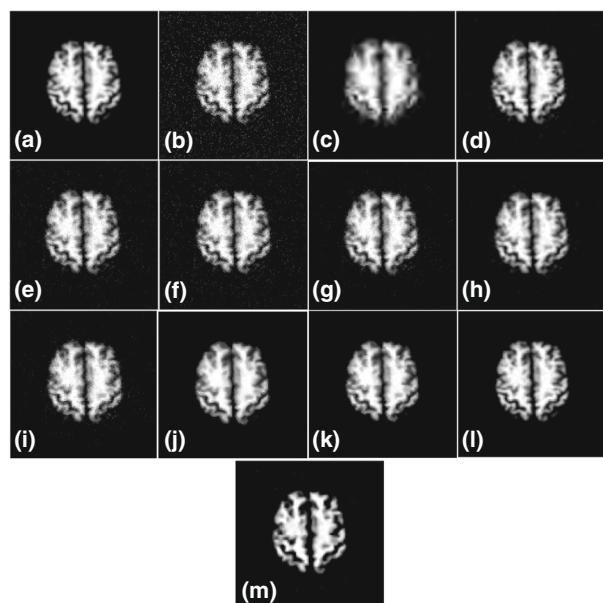


**Table 1** Metrics obtain for the Gaussian noisy brain PET (Fig. 5) image (noisy PSNR = 23 dB) and the denoised image with different denoising techniques

Methods	PSNR	Contrast	Edge value
Initial	23.52	0.8276	0.0440
VisuShrink [19]	26.73	0.7789	0.0403
BayesShrink [15]	32.19	0.8148	0.0554
NeighShrink [16]	28.50	0.8240	0.0589
ModineighShrink [34]	27.11	0.8237	0.0504
ModineighShrink [37]	32.16	0.8214	0.0506
Curvelet [46]	32.00	0.8143	0.0530
Wavelet Curvelet [29]	32.16	0.8207	0.0507
Non-Local Means Filter [9]	33.10	0.8231	0.0487
Vector Non-Local Means Filter [42]	34.39	0.8157	0.0432
Deep learning [23]	32.12	0.8420	0.0512
Proposed WNLMC	29.38	0.9775	0.0655

**Table 2** Metrics obtain for the Poisson (scale =  $1e15$ ) noisy brain PET (Fig. 6) image (noisy PSNR = 26 dB) and the denoised image with different denoising techniques

Methods	PSNR	Contrast	Edge value
Initial	25.12	0.2569	0.0217
VisuShrink [19]	26.32	0.2953	0.0323
BayesShrink [15]	26.32	0.2953	0.0323
NeighShrink [16]	26.32	0.2953	0.0323
ModineighShrink [34]	26.32	0.2953	0.0323
ModineighShrink [37]	26.32	0.2953	0.0323
Curvelet [46]	26.12	0.7809	0.0424
Wavelet Curvelet [29]	26.26	0.6809	0.0324
Non-Local Means Filter [9]	26.29	0.4965	0.0323
Vector Non-Local Means Filter [42]	28.24	0.4925	0.0318
Deep learning [23]	27.15	0.6285	0.0392
Proposed WNLMC	25.95	0.8196	0.0554

**Table 3** Metrics obtain for the mixed Gaussian-Poisson noise ( $1e15$ ) noisy brain PET (Fig. 7) image (noisy PSNR = 20 dB) and the denoised image with different denoising techniques

Methods	PSNR	Contrast	Edge value
Initial	20.31	0.7718	0.0622
VisuShrink [19]	25.13	0.8311	0.0372
BayesShrink [15]	23.77	0.8799	0.0453
NeighShrink [16]	24.34	0.8762	0.0528
ModineighShrink [34]	23.30	0.8835	0.0552
ModineighShrink [37]	24.44	0.8795	0.0480
Curvelet [46]	26.80	0.8764	0.0488
Wavelet Curvelet [29]	26.80	0.8764	0.0488
Non-Local Means Filter [9]	27.38	0.8767	0.0434
Vector Non-Local Means Filter [42]	28.15	0.8525	0.0413
Deep learning [23]	26.85	0.8720	0.0534
Proposed WNLMC	25.97	0.9825	0.0671

**Table 4** Metrics obtain for the the mixed Gaussian-Poisson noise ( $1e14$ ) noisy brain PET (Fig. 8) image (noisy PSNR = 26 dB) and the denoised image with different denoising techniques

Methods	PSNR	Contrast	Edge value
Initial	23.47	0.7556	0.0575
VisuShrink [19]	26.70	0.7860	0.0348
BayesShrink [15]	32.08	0.8076	0.0481
NeighShrink [16]	28.54	0.8069	0.0490
ModineighShrink [34]	27.13	0.8095	0.0514
ModineighShrink [37]	29.69	0.8084	0.0468
Curvelet [46]	31.87	0.8822	0.0454
Wavelet Curvelet [29]	31.87	0.8122	0.0454
Non-Local Means Filter [9]	30.85	0.8084	0.0422
Vector Non-Local Means Filter [42]	31.51	0.8045	0.0415
Deep learning [23]	31.85	0.8320	0.0534
Proposed WNLMC	29.17	0.9265	0.0705

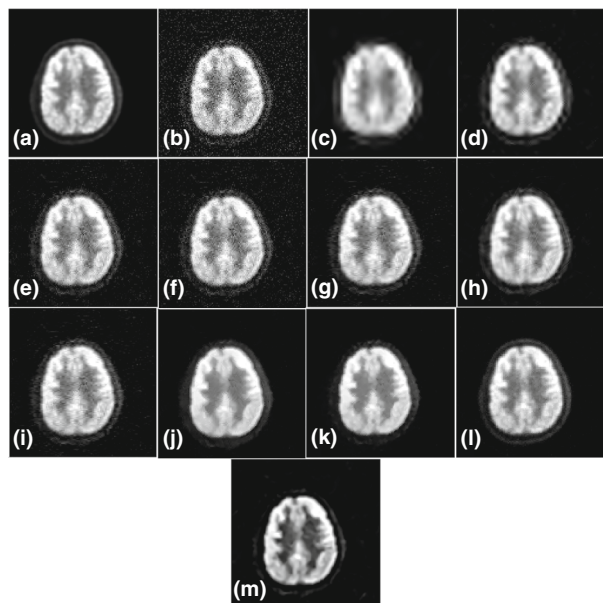
## 4.2 Results on clinical PET datasets

The experimental results of different denoising algorithms, including the proposed algorithm on clinical PET images with different noise levels are reported in this section. The original clinical PET, noisy version (Gaussian, Poisson and mixed Gaussian-Poisson) of PET and denoised images by different methods are shown in Figs. 9, 10, 11, 12 and 13. All numerical results are reported in Tables 5, 6, 7, 8 and 9, show that the proposed method generates better results than other methods for Gaussian noise (Fig. 9 and Table 5), Poisson noise (Figs. 10 and 11 and Tables 6 and 7) and mixed Gaussian-Poisson noise (Figs. 12 and 13 and Tables 8 and 9) with respect to contrast and edge value.

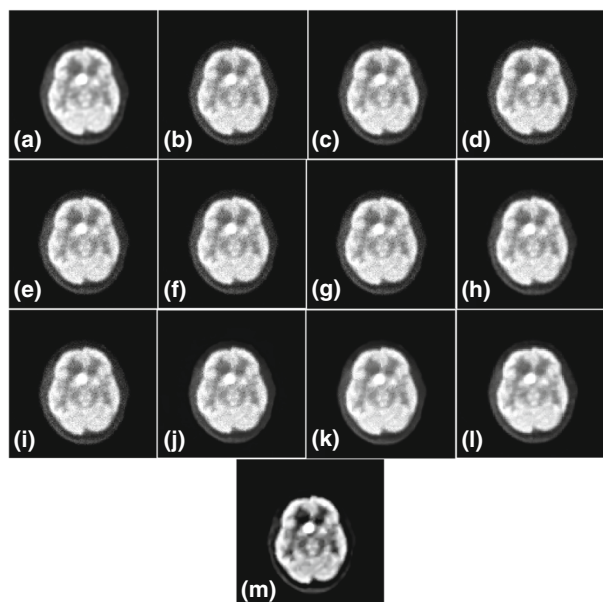
## 4.3 Comparative performance analysis among several denoising methods

Due to various physical degradation factors, contrast and the edge value of the PET image is very low that makes PET image denoising a challenging issue. Our main target to reconstruct the PET image in such a way that can preserve and improve the anisotropic details (edge and curve) and the contrast along with reduced noise level as much as possible. Generally, PSNR is used as a noise measurement parameter. The target of the denoising method is to reduce the noise level by improving the PSNR (higher PSNR) within the image. But sometimes it is noticed that the improvement of this parameter (PSNR) is not only an essential criteria to improve the quality of PET images for disease diagnosis. The higher PSNR may achieve good performance for homogeneous regions, but it may reduce the spatial resolution of denoised PET images. Such types of problems occur because of noise and spatial resolution are complementing each other, which makes PET image denoising a challenging issue. Additional measurements (metrics) such as edge value and contrast are the suitable one for measuring the quality of the denoised PET image for disease diagnosis. In this proposed method, we focus more on the restoring spatial resolution of PET image, so we try to improve the edge value and contrast of the denoised PET image. For that reason, instead of lower PSNR in the proposed method as compared to other methods, the proposed method achieves better performance in other metrics which is clearly reflected in the results of the proposed method.

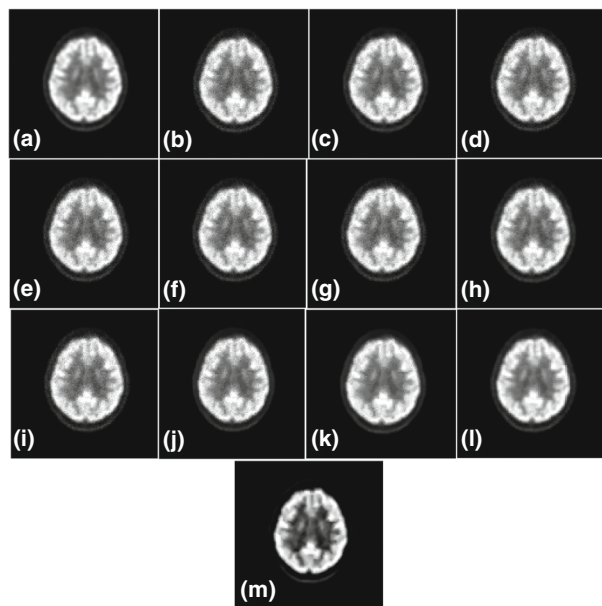
**Fig. 9** Performance comparison of various denoising techniques for Gaussian noise ( $\sigma = 200$ ) on clinical brain PET with PSNR = 23 dB. **a** Original, **b** noisy image, **c** VisuShrink [19], **d** BayesShrink [15], **e** NeighShrink [16], **f** ModineighShrink [34], **g** ModineighShrink [37], **h** Curvelet [46], **i** Wavelet curvelet [29], **j** Non-local means (NLM) [9], **k** Vector Non-local means [42], **l** Deep learning [23], **m** proposed wavelet curvelet NLM (WCNLM)



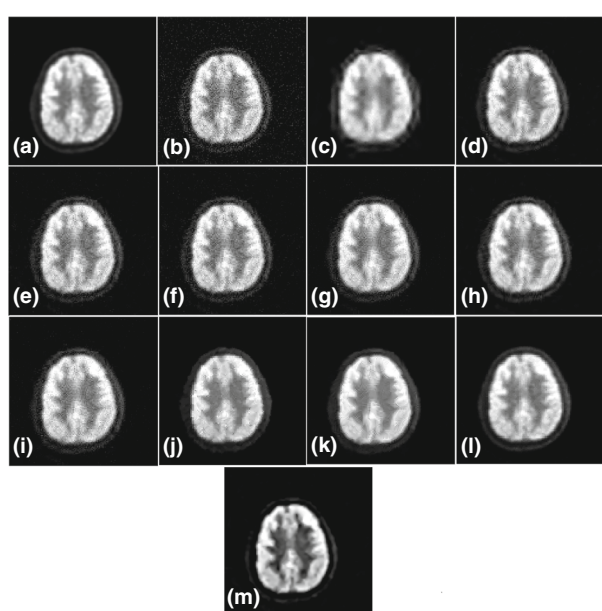
**Fig. 10** Performance comparison of various denoising techniques for Poisson noise ( $1e13$ ) on clinical brain PET with PSNR = 39 dB. **a** Original, **b** noisy image, **c** VisuShrink [19], **d** BayesShrink [15], **e** NeighShrink [16], **f** ModineighShrink [34], **g** ModineighShrink [37], **h** Curvelet [46], **i** Wavelet curvelet [29], **j** Non-local means (NLM) [9], **k** Vector Non-local means [42], **l** Deep learning [23], **m** proposed wavelet curvelet NLM (WCNLM)



**Fig. 11** Performance comparison of various denoising techniques for Poisson noise ( $1e14$ ) on clinical brain PET with PSNR = 30 dB. **a** Original, **b** noisy image, **c** VisuShrink [19], **d** BayesShrink [15], **e** NeighShrink [16], **f** ModineighShrink [34], **g** ModineighShrink [37], **h** Curvelet [46], **i** Wavelet curvelet [29], **j** Non-local means (NLM) [9], **k** Vector Non-local means [42], **l** Deep learning [23], **m** proposed wavelet curvelet NLM (WCNLM)



**Fig. 12** Performance comparison of various denoising techniques for mixed Gaussian ( $\sigma = 120$ ) - Poisson noise ( $1e13$ ) on simulated PET with PSNR = 26 dB. **a** Original, **b** noisy image, **c** VisuShrink [19], **d** BayesShrink [15], **e** NeighShrink [16], **f** ModineighShrink [34], **g** ModineighShrink [37], **h** Curvelet [46], **i** Wavelet curvelet [29], **j** Non-local means (NLM) [9], **k** Vector Non-local means [42], **l** Deep learning [23], **m** proposed wavelet curvelet NLM (WCNLM)



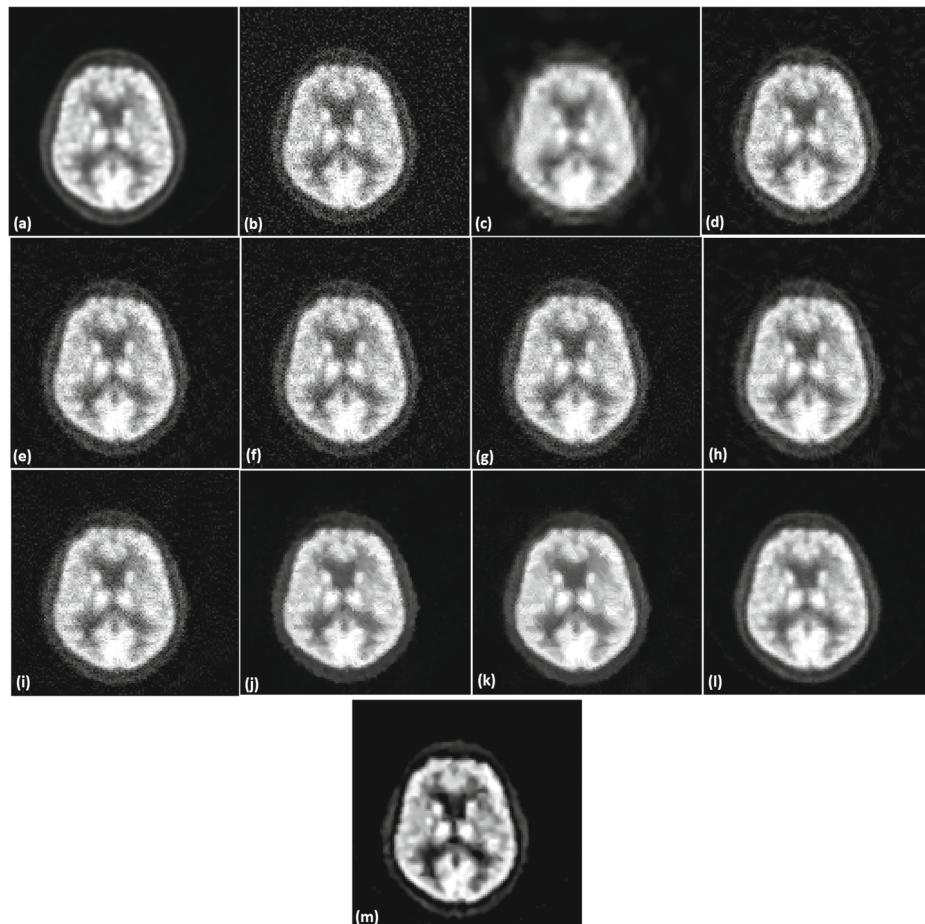


**Fig. 13** Performance comparison of various denoising techniques for mixed Gaussian ( $\sigma = 100$ ) - Poisson noise ( $1e13$ ) on simulated PET with PSNR = 24 dB. **a** Original, **b** Gaussian Noisy image, **c** VisuShrink [19], **d** BayesShrink [15], **e** NeighShrink [16], **f** ModineighShrink [34], **g** ModineighShrink [37], **h** Curvelet [46], **i** Wavelet curvelet [29], **j** Non-local means (NLM) [9], **k** Vector Non-local means [42], **l** Deep learning [23], **m** proposed wavelet curvelet NLM (WCNLM)

**Table 5** Metrics obtain for the Gaussian ( $\sigma = 200$ ) noisy brain PET (Fig. 9) image (noisy PSNR = 23 dB) and the denoised image with different denoising techniques

Methods	PSNR	Contrast	Edge value
Initial	23.57	0.7378	0.0507
VisuShrink [19]	28.47	0.4025	0.0339
BayesShrink [15]	31.51	0.5920	0.0393
NeighShrink [16]	29.19	0.6921	0.0496
ModineighShrink [34]	27.57	0.7095	0.0524
ModineighShrink [37]	30.86	0.6765	0.0469
Curvelet [46]	33.04	0.6305	0.0430
Wavelet Curvelet [29]	30.86	0.6767	0.0468
Non-Local Means Filter [9]	33.97	0.6308	0.0371
Vector Non-Local Means Filter [42]	34.85	0.6296	0.0367
Deep learning [23]	32.97	0.7308	0.0411
Proposed WCNLM	30.12	0.8409	0.0674

**Table 6** Metrics obtain for the Poisson (scale =  $1e13$ ) noisy brain PET (Fig. 10) image (noisy PSNR = 39dB) and the denoised image with different denoising techniques

Methods	PSNR	Contrast	Edge value
Initial	39.17	0.7455	0.0186
VisuShrink [19]	40.30	0.7918	0.0179
BayesShrink [15]	39.17	0.8511	0.0186
NeighShrink [16]	39.24	0.8310	0.0184
ModineighShrink [34]	39.23	0.8487	0.0184
ModineighShrink [37]	39.28	0.8221	0.0181
Curvelet [46]	39.28	0.8214	0.0181
Wavelet Curvelet [29]	41.10	0.8107	0.0182
Non-Local Means Filter [9]	41.96	0.7945	0.0171
Vector Non-Local Means Filter [42]	42.87	0.7852	0.0180
Deep learning [23]	41.51	0.8132	0.0185
Proposed WNLMC	39.14	0.9361	0.0236

**Table 7** Metrics obtain for the Poisson (scale =  $1e14$ ) noisy brain PET (Fig. 11) image (noisy PSNR = 30 dB) and the denoised image with different denoising techniques

Methods	PSNR	Contrast	Edge value
Initial	30.44	0.7981	0.0464
VisuShrink [19]	32.82	0.5614	0.0338
BayesShrink [15]	36.58	0.6624	0.0383
NeighShrink [16]	35.25	0.7684	0.0414
ModineighShrink [34]	33.95	0.7775	0.0426
ModineighShrink [37]	35.30	0.7728	0.0395
Curvelet [46]	35.30	0.7721	0.0395
Wavelet Curvelet [29]	35.30	0.7721	0.0395
Non-Local Means Filter [9]	36.14	0.7246	0.0398
Vector Non-Local Means Filter [42]	37.74	0.7159	0.0388
Deep learning [23]	37.97	0.7532	0.0410
Proposed WNLMC	34.87	0.8757	0.0640

**Table 8** Metrics obtain for the mixed Gaussian ( $\sigma = 120$ ) - Poisson noise ( $1e13$ ) noisy brain PET (Fig. 12) image (noisy PSNR = 26 dB) and the denoised image with different denoising techniques

Methods	PSNR	Contrast	Edge value
Initial	26.85	0.6444	0.0481
VisuShrink [19]	30.60	0.5311	0.0338
BayesShrink [15]	32.88	0.7459	0.0389
NeighShrink [15]	30.91	0.7759	0.0414
ModineighShrink [34]	29.86	0.7884	0.0431
ModineighShrink [37]	31.15	0.8021	0.0372
Curvelet [46]	33.37	0.7423	0.0397
Wavelet Curvelet [29]	31.15	0.7724	0.0372
Non-Local Means Filter [9]	33.98	0.7418	0.0346
Vector Non-Local Means Filter [42]	34.12	0.7389	0.0336
Deep learning [23]	34.51	0.7532	0.0410
Proposed WNLMC	31.79	0.8643	0.0569

**Table 9** Metrics obtain for the the mixed Gaussian ( $\sigma = 100$ ) - Poisson noise ( $1e13$ ) noisy brain PET (Fig. 13) image (noisy PSNR = 24 dB) and the denoised image with different denoising techniques

Methods	PSNR	Contrast	Edge value
Initial	24.53	0.6136	0.0556
VisuShrink [19]	28.50	0.4295	0.0374
BayesShrink [15]	30.28	0.6571	0.0468
NeighShrink [16]	28.55	0.6758	0.0483
ModineighShrink [34]	27.48	0.6896	0.0500
ModineighShrink [37]	28.44	0.6785	0.0457
Curvelet [46]	31.43	0.6746	0.0443
Wavelet Curvelet [29]	31.43	0.6746	0.0443
Non-Local Means Filter [9]	32.63	0.6706	0.0409
Vector Non-Local Means Filter [42]	33.52	0.6698	0.0401
Deep learning [23]	33.74	0.6920	0.0452
Proposed WNLMC	29.77	0.7910	0.0679

The results of the different denoising methods are shown in previous sections with respect to visual perceptive (Figs. 5–13) and different metrics, such as PSNR, contrast and edge value (Tables 1–9). It is observed that all numerical values (contrast and edge value) except PSNR indicate the advantage of the proposed method as compared to the other methods.

The results in Sections 4.1 and 4.2 showed that universal threshold based method (VisuShrink) produces blur images due to the removal of too much wavelet coefficients, which is reflected in Figs. 5, 7 and 8 for simulated phantom and Figs. 9, 12 and 13 for clinical PET images. This type of problem is overcome by a soft adaptive threshold called BayesShrink, which is reported in Tables 1–9. The experimental results in Tables 1–9 showed that NeighShrink [16] achieved better results than VisuShrink due to the utilization of the neighborhood characteristic. A modification of NeighShrink was proposed by Mohideen et al. [34] in order to restrict the suppression of many details of wavelet coefficients. It is experimentally observed that ModineighShrink [34] fails to achieve better results than NeighShrink for PET image denoising with respect to PSNR. Another modification of NeighShrink in Ref. [37] incorporated the size of wavelet subband during thresholding and achieved better performance than NeighShrink, which is reported in Tables 1–9. Although the curvelet-based denoising [46] method achieved promising results for anisotropic features, but it does not provide an optimal representation for the small isotropic features as compared to wavelet-based denoising. In Ref. [29], Pogam et al. combines the wavelet and curvelet to handle both isotropic and anisotropic features. Although their method improves the PSNR over individual wavelet and curvelet-based method, but did not achieve significant improvement with respect to the medical point of view. Whereas NLM [9] based method performs well to handle the structural details but it reduces the contrast level and takes larger computation time than other methods. It is experimentally observed that the vector based NLM method proposed by Said et al. [42] achieved promising results over NLM depending with respect to PSNR on the simulated and clinical PET database for Gaussian noisy PET images, but did not achieve significant improvement with respect to the medical point of view.

The wavelet-only, curvelet-only and wavelet-curvelet based denoising methods improve the PSNR but fail to improve the contrast and edge value. These methods are not well suited in diseases diagnosis, such as precise tumor region identification (visual and numerical) (see Section 4.6), which are the main desirable requirement for PET image denoising. The denoising method proposed by Pogam et al. [29] used a combination of wavelet and curvelet using the wavelet coefficient thresholding technique. It is experimentally observed that the method proposed by Pogam et al. achieved better results than wavelet-only and curvelet-only based denoising methods. It is also observed that thresholding of wavelet coefficients improves the PSNR value by filtering the noise in wavelet coefficients, but sometimes it is not good enough for handling the anisotropic features. The presence of thresholding in Ref. [29] removes the important image details such as edges along with noise in the denoised image due to the suppression of many wavelet coefficients, which is clearly reflected in the numerical values of the denoised image. In order to avoid such situation, we do not use the thresholding of wavelet coefficients. Qualitatively, a notable gain is achieved in the proposed denoised PET images in terms of contrast enhancement than the method proposed by Pogam et al. On the other hand, the method in Ref. [29] is computationally expensive because thresholding of wavelet coefficients of a particular scale depends on the next coarser scale. Said et al. [42] applied their proposed method (vector non-local means) on the Gaussian noisy datasets. Generally, Poisson and mixed Gaussian-Poisson noises are present in PET dataset instead of Gaussian noise. The experimental results show that when PET images contains Poisson (Figs. 6, 10 and 11 and Tables 2, 6 and 7) and mixed Gaussian-Poisson (Figs. 7, 8, 12, 13 and Tables 3, 4, 8 and 9), improvements of the proposed denoising method are better than the method proposed by Pogam et al. and Said et al. From the experimental results, it is observed that, the deep learning based method in Ref. [23] achieves better performance over almost all other methods except the proposed method. The proposed method properly handles both isotropic and anisotropic features over the deep learning based method described in Ref. [23] which is clearly reflected in numerical results and visual outputs. Generally, the deep neural network produces promising results in image denoising when the noise level in test datasets is approximately similar to the noise level in training datasets. On the other hand, the performance of the deep learning is reduced in cases of insufficient number of training images.

It is also experimentally observed that the contrast and edge value of the proposed denoised PET images (simulated phantom and clinical PET) are much better than the other denoised PET images, which is clearly reflected in the numerical values in Tables 1–9. The denoised PET image by proposed method significantly helps in medical applications, such as segmentation of gray matter (Figs. 19 and 20) and precise tumor region identification (visual and numerical) (Figs. 21 and 22). All the results are verified by the neurologist.

#### 4.4 Noise level versus contrast and edge value

In this section, noise level versus contrast and edge value are measured by considering PET images of 100 patients. Noise level ( $\sigma$ ) versus contrast and edge value are plotted in Figs. 14 and 15 respectively, where x-axis denotes the noise level (sigma) and the y-axis denotes contrast (Fig. 14) and edge value (Fig. 15). In Figs. 14 and 15, contrast and edge values of the proposed method for different noise levels are plotted by the red curve. From the Figs. 14 and 15, it is observed that the proposed method achieves better (higher) contrast and edge values than the other methods for different noise levels. The average contrast and

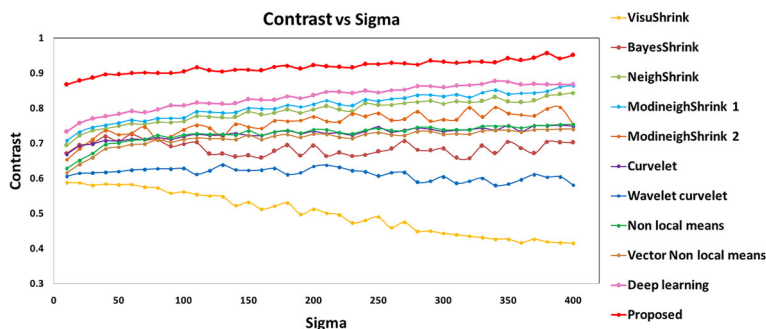


**Fig. 14** Sigma ( $\sigma$ ) versus contrast for different denoising methods, including proposed method

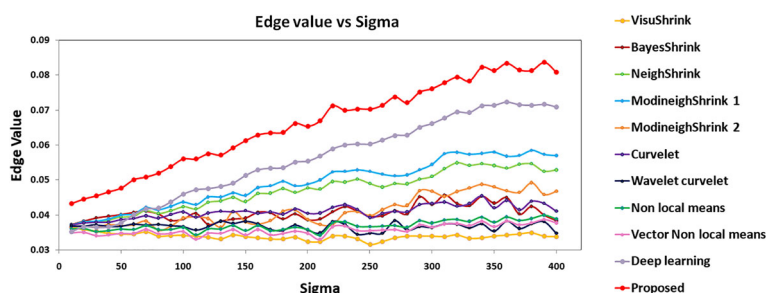


**Fig. 15** Sigma ( $\sigma$ ) versus edge value for different denoising methods, including proposed method

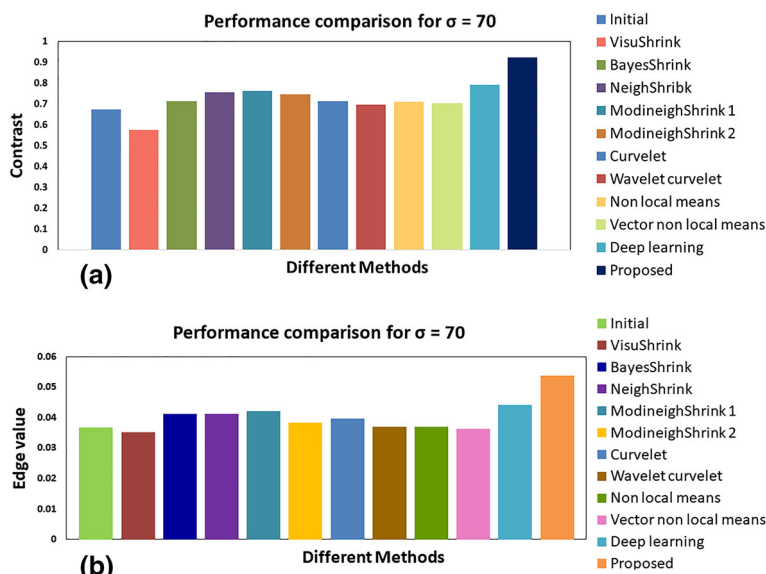


**Fig. 16** Performance evaluation of different methods for  $\sigma = 70$ . **a** Average contrast of different denoising methods, **b** average edge value of different denoising methods

edge value of each denoising method for sigma ( $\sigma$ ) = 70 are shown in Figs. 16a and 16b respectively.

#### 4.5 Time measurement of different denoising methods

The average computational time (in seconds) requirement of our proposed method and other methods [9, 15, 16, 19, 23, 29, 34, 37, 42, 46] is discussed in this section with different noise levels ( $\sigma = 100, 120, 150$  and  $200$ ), which is shown in Fig. 17. The execution time (in second) mentioned in Fig. 17 refers the time to compute different methods excluding the input-output (I/O) operation. Although BayesShrink [15] achieves better performance than VisuShrink [19] with respect to several metrics, but BayesShrink is more computationally expensive than VisuShrink due to the adaptive threshold. It is experimentally observed that due to the utilization of neighborhood coefficients, NeighShrink [16] takes larger time than VisuShrink. Modification of NeighShrink (ModineighShrink) in Ref. [34, 37] requires larger computation time as compared to NeighShrink, which is reflected in Fig. 17. It is experimentally observed that due to the integration of multiple methods, the proposed method the method proposed in Ref. [29] take relatively more execution time than the individual wavelet and curvelet based methods. The average execution time requirement of the proposed method is almost similar to Pogam et al. [29] method. It is also observed that the time requirement of non-local means (NLM) is much higher than other methods due to its computational cost. It is experimentally observed that, vector based non-local means in Ref [42] reduces the average execution time (Fig. 17) non-local means by considering only those pixels which are most similar to each other using a probabilistic approach. Proposed method reduces the computational time of non-local means (NLM) by selecting the similar patches in advance using K-means based tree clustering. In the proposed method, the average percentage (%) of time taken for building a cluster tree with respect to the overall computation time is shown in Fig. 18. Although the deep learning based method in Ref. [23] achieves promising results in denoising, but the average computational time of the method in Ref. [23] is much larger than other methods, which is shown in Fig. 17. The time taken by deep learning based method [23] highlighted in Fig. 18 refers the time to denoise each slice during the testing phase.

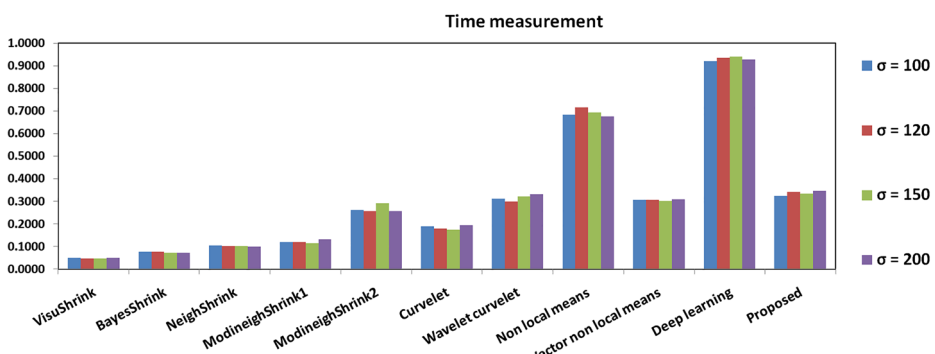


**Fig. 17** Performance analysis between proposed and existing methods with respect to average time requirement in seconds for different noise levels

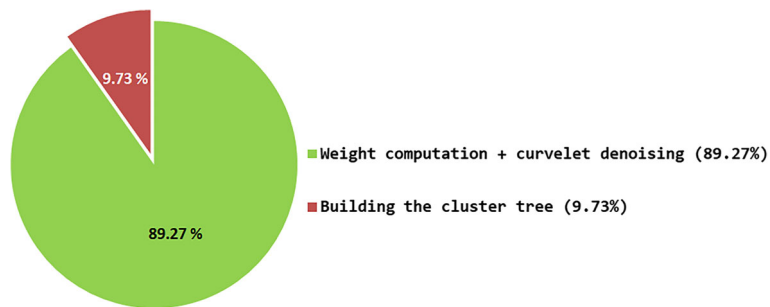
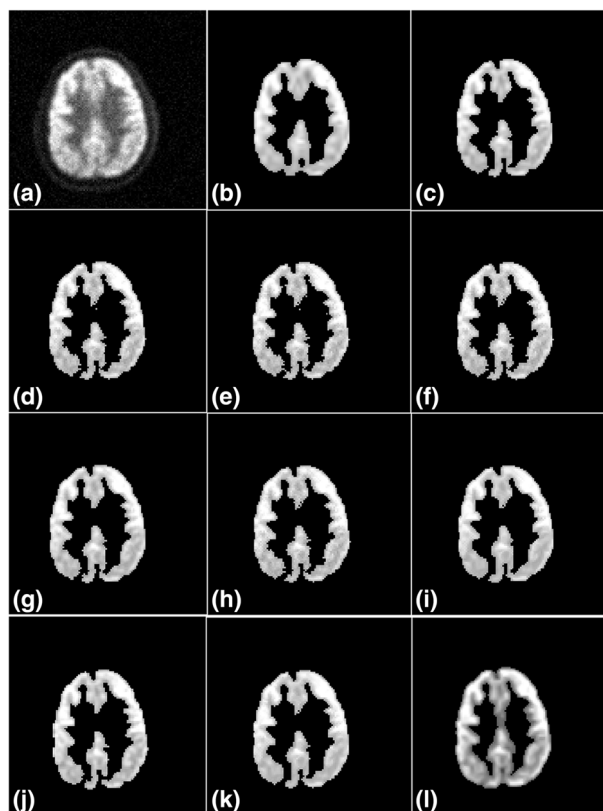


**Fig. 18** Percentage (%) of time taken for building a cluster tree and patch weight computation + curvelet denoising

#### 4.6 Applications of proposed denoising method in medical domain

PET image denoising is one of the important pre-processing steps [5] for facilitating the further medical applications such as gray matter segmentation and, and precise tumor region

**Fig. 19** Gray matter segmentation results on different denoised PET images. **a** noisy image, **b** VisuShrink [19], **c** BayesShrink [15], **d** NeighShrink [16], **e** ModineighShrink [34], **f** ModineighShrink [37], **g** Curvelet [46], **h** Wavelet curvelet [29], **i** Non-local means (NLM) [9], **j** Vector Non-local means [42], **k** Deep learning [23], **l** proposed wavelet curvelet NLM (WCNLM)



identification (numerical results and visual outputs). Generally, PSNR is used as a noise measurement parameter. But sometimes it is noticed that the improvement of this parameter fails to demonstrate the direct link to improve the disease diagnosis. In the proposed method, contrast and edge value are used along with PSNR for measuring the performance of the proposed method over other methods. To show the effectiveness of the proposed denoising method, the present work analyses two medical applications such as precise tumor region identification and gray matter segmentation (numerical results and visual outputs) of the different denoised PET images and highlight the differences between proposed method and other denoising methods.

To measure the performance of the different denoising methods, gray matter segmentation [6] technique using fuzzy c-means has been applied on the denoised image produced by the proposed method and other methods. Figs. 19 and 20 show the gray matter segmentation results on the different denoised PET images. Here, fifteen (15) features [27, 32, 53] have been used for gray matter segmentation [5, 6], such as the gray value, mean, min, max, median, standard deviation, median of absolute deviation from the median (MAD), probability, variance using probability, ROAD factor, absolute energy, skewness, kurtosis, homogeneity, and edge value. The usefulness of these features in this purpose is tested experimentally for PET image analysis. The visual results in the Figs. 19 and 20 show

**Fig. 20** Gray matter segmentation results on different denoised PET images. **a** noisy image, **b** VisuShrink [19], **c** BayesShrink [15], **d** NeighShrink [16], **e** ModineighShrink [34], **f** ModineighShrink [37], **g** Curvelet [46], **h** Wavelet curvelet [29], **i** Non-local means (NLM) [9], **j** Vector Non-local means [42], **k** Deep learning [23], **l** proposed wavelet curvelet NLM (WCNLM)

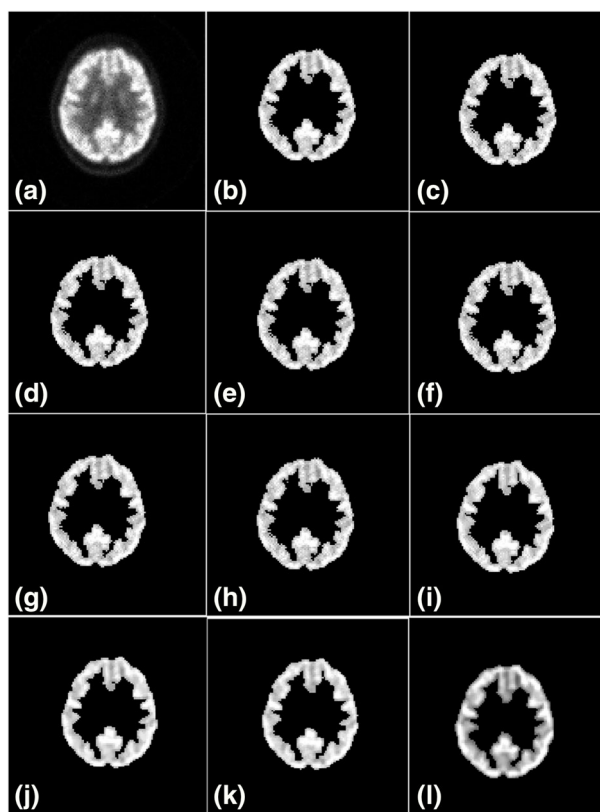
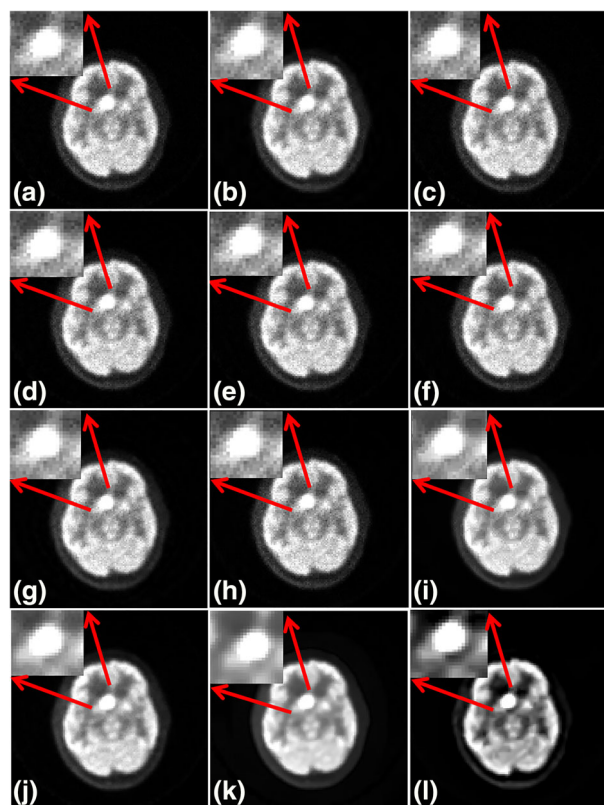


**Fig. 21** Tumor regions highlight on different denoised PET images. **a** noisy image (PSNR = 39 dB), **b** VisuShrink [19], **c** BayesShrink [15], **d** NeighShrink [16], **e** ModineighShrink [34], **f** ModineighShrink [37], **g** Curvelet [46], **h** Wavelet curvelet [29], **i** Non-local means (NLM) [9], **j** Vector Non-local means [42], **k** Deep learning [23], **l** proposed wavelet curvelet NLM (WCNLM)



that gray matter segmentation (Figs. 19j and 20j) using proposed denoised PET images are superior than the other denoising methods (Figs. 19b-i and 20b-i). The different denoising methods [9, 15, 16, 19, 23, 29, 34, 37, 42, 46] create discontinuous edges along the boundary region of the segmented gray matter (Figs. 19b-i and 20b-i) as compared to the segmented results (Figs. 19j and 20j) using our denoising method.

In order to measure the performance of the different denoising methods for precise tumor region identification (numerical results and visual outputs) [5], several metrics values are evaluated around the tumor region of the denoised PET images produced by the proposed method and other methods. The visual results in Figs. 21 and 22 show the performance of the proposed method along with other denoising methods on the noisy tumor regions. The visual quality of tumor region of the denoised PET images obtained by the proposed method (Figs. 21j and 22j) is much superior than the other denoising methods (Figs. 21a-i and 22a-i). The numerical results in Tables 10 and 11 show different metrics value of the tumor regions using the proposed method and others methods. These results show that although the proposed method does not improve the PSNR around the tumor region as compared to other methods, but it significantly improves the contrast and edge value, which helps during tumor analysis.

**Fig. 22** Tumor regions highlight on different denoised PET image.  
**a** noisy image (PSNR = 32 dB),  
**b** VisuShrink [19],  
**c** BayesShrink [15],  
**d** NeighShrink [16],  
**e** ModineighShrink [34],  
**f** ModineighShrink [37],  
**g** Curvelet [46], **h** Wavelet curvelet [29], **i** Non-local means (NLM) [9], **j** Vector Non-local means [42], **k** Deep learning [23], **l** proposed wavelet curvelet NLM (WCNLssM)

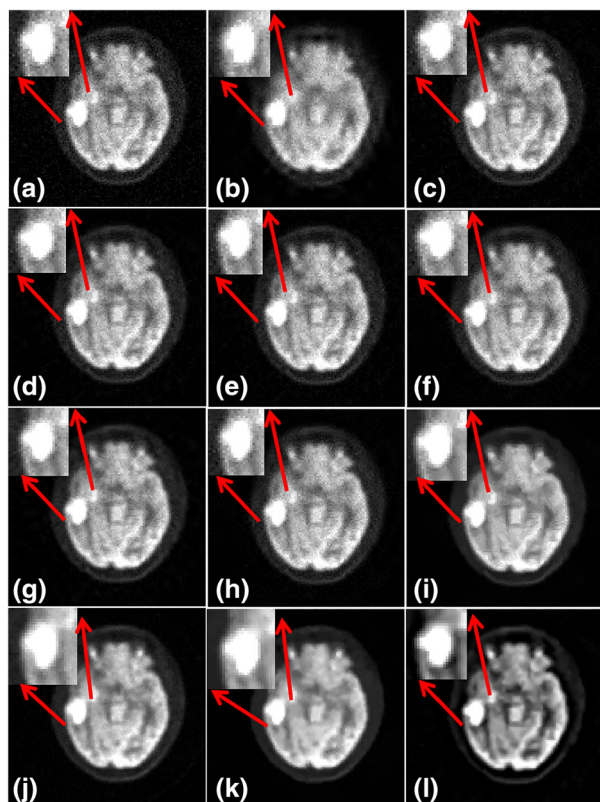


**Table 10** Metrics obtain for the noisy (PSNR = 39 dB) tumor region (Fig. 21a) and the denoised tumor regions (Fig. 21b-i) with different denoising techniques

Methods	PSNR	Contrast	Edge value
Initial	37.17	0.7455	0.0186
VisuShrink [19]	40.30	0.7918	0.0179
BayesShrink [15]	39.17	0.8511	0.0186
NeighShrink [16]	39.24	0.8310	0.0184
ModineighShrink [34]	39.23	0.8487	0.0184
ModineighShrink [37]	39.28	0.8221	0.0181
Curvelet [46]	39.28	0.8214	0.0181
Wavelet Curvelet [29]	41.10	0.8107	0.0182
Non-Local Means Filter [9]	41.96	0.7945	0.0171
Vector Non-Local Means Filter [42]	42.52	0.7952	0.0182
Deep learning [23]	41.21	0.8120	0.0232
Proposed WNLMC	38.15	0.9561	0.0336

**Table 11** Metrics obtain for the noisy ( $\text{PSNR} = 32 \text{ dB}$ ) tumor region (Fig. 22a) and the denoised tumor regions (Fig. 22b-i) with different denoising techniques

Methods	PSNR	Contrast	Edge value
Initial	32.36	0.7544	0.0269
VisuShrink [9]	32.99	0.5883	0.0190
BayesShrink [15]	35.46	0.7194	0.0238
NeighShrink [16]	35.72	0.7226	0.0232
ModineighShrink [34]	34.90	0.7339	0.0240
ModineighShrink [37]	35.84	0.7179	0.0216
Curvelet [46]	37.15	0.6947	0.0225
Non-Local Means Filter [9]	36.33	0.6763	0.0201
Vector Non-Local Means Filter [42]	37.21	0.6712	0.0221
Deep learning [23]	36.11	0.7420	0.0262
Proposed WNLMC	34.51	0.8964	0.0382

## 5 Conclusion and future scope

Denoising is a pre-processing technique that can improve the PET image qualities for further processing such as segmentation. The aim of the present work is to investigate a proper denoising technique for PET images. Towards this goal, this paper proposes an efficient PET image denoising technique based on the combination multi-scale transform (wavelet and curvelet) and tree clustering non-local means (TNLM). The proposed method can handle different type of noises (Gaussian or Poisson or mixed Gaussian-Poisson) while preserving and enhancing the image features, such as edges and contrast. Proposed denoising method overcomes the limitations that are encountered in individual wavelet, curvelet, non-local means, vector non-local means and deep learning based denoising techniques. The improved performance is achieved due to the proper integration of multiple methods that can significantly help in medical applications such as gray matter segmentation and precise tumor region identification.

The present method was tested on the clinical dataset provided by Apollo Gleneagles Hospital, Kolkata, India and synthetic brain PET phantom reference images which are downloaded from <http://depts.washington.edu/petcdro>. The future aim is to test the proposed method on several PET datasets for extensive analysis of the results. Furthermore, our target is to extend our proposed work by analyzing various types of dementias like Alzheimer's disease, Dementia with Lewy bodies (DLB) and Parkinson's disease on the proposed denoised PET images.

**Acknowledgment** This research work was supported by the Board of Research in Nuclear Sciences (BRNS), DAE, Government of India, under the Reference No. 34/14/13/2016-BRNS/34044. Sincere gratitude to Dr. Punit Sharma, MD at Apollo Gleneagles Hospital, Kolkata, India for providing the clinical PET brain datasets and valuable comments throughout this work. The authors would like to thank Dr. Haseeb Hassan, MD, DM at Rabindranath Tagore International Institute of Cardiac Sciences, Kolkata, India, and Dr. Arindam Chatterjee, MD, at Variable Energy Cyclotron Centre (VECC), Kolkata, India for their helpful comments. The authors would like to thank the referees for providing their very valuable comments on the original version of the manuscript.

## References

1. Alessio AM, Kinahan PE (2006) Improved quantitation for pet/ct image reconstruction with system modeling and anatomical priors. *Med Phys* 33(11):4095–4103
2. AlZubi S, Islam N, Abbot M (2011) Multiresolution analysis using wavelet, ridgelet, and curvelet transforms for medical image segmentation. *J Biomed Imaging* 2011:4
3. Bal A, Banerjee M, Chakrabarti A, Sharma P (2018) MRI brain tumor segmentation and analysis using rough-fuzzy C-Means and shape based properties. *Journal of King Saud University-Computer and Information Sciences*
4. Bal A, Banerjee M, Sharma P, Maitra M (2018) Brain tumor segmentation on MR image using k-means and fuzzy-possibilistic clustering. In: 2018 2nd international conference on electronics, materials engineering & Nano-Technology (IEMENTech), pp 1–8
5. Bal A, Banerjee M, Sharma P, Maitra M (2019) An efficient wavelet and curvelet-based pet image denoising technique. *Med Biol Eng Comput* 57(12):2567–2598
6. Bal A, Banerjee M, Sharma P, Maitra M (2020) Gray matter segmentation and delineation from positron emission tomography (pet) image. In: Emerging technology in modelling and graphics. Springer, pp 359–372
7. Beghdadi A, Le Negrate A (1989) Contrast enhancement technique based on local detection of edges. *Comput Vis Graph Image Process* 46(2):162–174
8. Brox T, Kleinschmidt O, Cremers D (2008) Efficient nonlocal means for denoising of textural patterns. *IEEE Trans Image Process* 17(7):1083–1092
9. Buades A, Coll B, Morel J-M (2005) A non-local algorithm for image denoising. In: 2005. CVPR 2005. IEEE Computer Society Conference on Computer Vision and Pattern Recognition, vol 2, IEEE, pp 60–65
10. Buades A, Coll B, Morel J-M (2005) A review of image denoising algorithms, with a new one. *Multiscale Model Simul* 4(2):490–530
11. Cai TT, Silverman BW (2001) Incorporating information on neighbouring coefficients into wavelet estimation, *sankhyā: The Indian Journal of Statistics Series B*, pp 127–148
12. Candès EJ, Donoho DL (2004) New tight frames of curvelets and optimal representations of objects with piecewise  $c_2$  singularities. *Commun Pure Appl Math* 57(2):219–266
13. Candès E, Demanet L, Donoho D, Ying L (2006) Fast discrete curvelet transforms. *Multiscale Model Simul* 5(3):861–899
14. Chang SG, Yu B, Vetterli M (1998) Spatially adaptive wavelet thresholding with context modeling for image denoising. In: 1998. ICIP 98. Proceedings. 1998 International Conference on Image Processing, vol 1, IEEE, pp 535–539
15. Chang SG, Yu B, Vetterli M (2000) Adaptive wavelet thresholding for image denoising and compression. *IEEE Trans Image Process* 9(9):1532–1546
16. Chen G, Bui TD, Krzyzak A (2005) Image denoising using neighbouring wavelet coefficients. *Integr Comput-Aided Eng* 12(1):99–107
17. Christian BT, Vandehey NT, Floberg JM, Mistretta CA (2010) Dynamic pet denoising with hpr processing, *Journal of nuclear medicine: official publication. Soc Nuclear Med* 51(7):1147
18. Cui J, Gong K, Guo N, Wu C, Meng X, Kim K, Zheng K, Wu Z, Fu L, Xu B et al (2019) Pet image denoising using unsupervised deep learning. *Eur J Nuclear Med Mol Imaging* 46(13):2780–2789
19. Donoho DL, Johnstone IM (1994) Ideal spatial adaptation by wavelet shrinkage, *biometrika*, pp 425–455
20. Donoho DL (1995) De-noising by soft-thresholding. *IEEE Trans Inf Theory* 41(3):613–627
21. Dutta J, Leahy RM, Li Q (2013) Non-local means denoising of dynamic pet images. *PloS one* 8(12):e81390
22. Ellis S, Mallia A, McGinnity CJ, Cook GJ, Reader AJ (2018) Multitracer guided pet image reconstruction. *IEEE Trans Rad Plasma Med Sci* 2(5):499–509
23. Gong K, Guan J, Liu C-C, Qi J (2018) Pet image denoising using a deep neural network through fine tuning. *IEEE Trans Radiat Plasma Med Sci* 3(2):153–161
24. Green GC (2005) Wavelet-based denoising of cardiac PET data. Carleton University
25. Huerga C, Castro P, Corredoira E, Coronado M, Delgado V, Guibelalde E (2017) Denoising of pet images by context modelling using local neighbourhood correlation. *Phys Med Biol* 62(2):633
26. Hyder SA, Sukanesh R (2011) An efficient algorithm for denoising mr and ct images using digital curvelet transform. In: Software Tools and Algorithms for Biological Systems. Springer, pp 471–480
27. Kekre H, Gharge S (2010) Texture based segmentation using statistical properties for mammographic images. *Entropy* 1:2

28. Kervrann C, Boulanger J, Coupé P (2007) Bayesian non-local means filter, image redundancy and adaptive dictionaries for noise removal. In: International conference on scale space and variational methods in computer vision. Springer, pp 520–532
29. Le Pogam A, Hanzouli H, Hatt M, Le Rest CC, Visvikis D (2013) Denoising of pet images by combining wavelets and curvelets for improved preservation of resolution and quantitation. *Med Image Anal* 17(8):877–891
30. Luisier F, Blu T, Unser M (2007) A new sure approach to image denoising: Interscale orthonormal wavelet thresholding. *IEEE Trans Image Process* 16(3):593–606
31. Mahmoudi M, Sapiro G (2005) Fast image and video denoising via nonlocal means of similar neighborhoods. *IEEE Signal Process Lett* 12(12):839–842
32. Maji P, Pal SK (2011) Rough-fuzzy pattern recognition: applications in bioinformatics and medical imaging, vol. 3. Wiley, New York
33. Mejia JM, Domínguez HdJO, Villegas OOV, Mányez LO, Mederos B (2014) Noise reduction in small-animal pet images using a multiresolution transform. *IEEE Trans med Imaging* 33(10):2010–2019
34. Mohideen SK, Perumal SA, Sathik MM (2008) Image de-noising using discrete wavelet transform. *Int J Comput Sci Netw Secur* 8(1):213–216
35. Mohl B, Wahlberg M, Madsen P (2003) Ideal spatial adaptation via wavelet shrinkage. *J Acoust Soc Amer* 114:1143–1154
36. Nguyen V-G, Lee S-J (2010) Nonlocal-means approaches to anatomy-based pet image reconstruction. In: 2010 IEEE Nuclear science symposium conference record (NSS/MIC). IEEE, pp 3273–3277
37. Om H, Biswas M (2012) An improved image denoising method based on wavelet thresholding. *J Signal Inf Proces* 3(01):109
38. Peter DJ, Govindan V, Mathew AT (2010) Nonlocal-means image denoising technique using robust m-estimator. *J Comput Sci Technol* 25(3):623–631
39. Qi J, Leahy RM (1999) A theoretical study of the contrast recovery and variance of map reconstructions from pet data. *IEEE Trans Med Imaging* 18(4):293–305
40. Qi J, Leahy RM (2000) Resolution and noise properties of map reconstruction for fully 3-d pet. *IEEE Trans Med Imaging* 19(5):493–506
41. RIDGELETS E (1998) Ridgelets: theory and applications, Ph.D. thesis, Ph. D. thesis, Stanford University, USA
42. Said AB, Hadjidj R, Melkemi KE, Foufou S (2016) Multispectral image denoising with optimized vector non-local mean filter. *Digital Signal Process* 58:115–126
43. Shalchian B, Rajabi H, Soltanian-Zadeh H (2009) Assessment of the wavelet transform in reduction of noise from simulated pet images. *J Nuclear Med Technol* 37(4):223–228
44. Shidahara M, Ikoma Y, Kershaw J, Kimura Y, Naganawa M, Watabe H (2007) Pet kinetic analysis: wavelet denoising of dynamic pet data with application to parametric imaging. *Ann Nuclear Med* 21(7):379–386
45. Shih Y-Y, Chen J-C, Liu R-S (2005) Development of wavelet de-noising technique for pet images. *Comput Med Imaging Graph* 29(4):297–304
46. Starck J-L, Candès EJ, Donoho DL (2002) The curvelet transform for image denoising. *IEEE Trans Image Process* 11(6):670–684
47. Starck J-L, Murtagh F, Fadili JM (2010) Sparse image and signal processing: wavelets, curvelets, morphological diversity. Cambridge University Press
48. Taswell C (2000) The what, how, and why of wavelet shrinkage denoising. *Comput Sci Eng* 2(3):12–19
49. Turkheimer FE, Banati RB, Visvikis D, Aston JA, Gunn RN, Cunningham VJ (2000) Modeling dynamic pet-spect studies in the wavelet domain. *J Cereb Blood Flow Metabol* 20(5):879–893
50. Wang G, Qi J (2014) Pet image reconstruction using kernel method. *IEEE Trans Med Imaging* 34(1):61–71
51. Wink AM, Roerdink JB (2004) Denoising functional mr images: a comparison of wavelet denoising and gaussian smoothing. *IEEE Trans Med Imaging* 23(3):374–387
52. Xu Z, Bagci U, Seidel J, Thomasson D, Solomon J, Mollura DJ (2014) Segmentation based denoising of pet images: An iterative approach via regional means and affinity propagation, in: International Conference on Medical Image Computing and Computer-Assisted Intervention. Springer, pp 698–705
53. Yang H-Y, Wang X-Y, Wang Q-Y, Zhang X-J (2012) Ls-svm based image segmentation using color and texture information. *J Vis Commun Image Represent* 23(7):1095–1112



**Abhishek Bal** received his B.Sc. degree in Computer Science from West Bengal State University, Kolkata, India in 2012, M.Sc. (2014) degree in Computer Science from the University of Calcutta, Kolkata, India and M.Tech. (2016) degree in Computer Science and Engineering from the West Bengal University of Technology, Kolkata, India. He worked as a research fellow at RCC Institute of Information Technology, Kolkata under the Board of Research in Nuclear Sciences (BRNS), DAE, Government of India. Presently he is a research scholar at the department of Information Technology in the A.K.Choudhury School of Information Technology, University of Calcutta, Kolkata, India. His current research interests include medical image processing, machine learning and handwriting analysis. He has published several research papers in referred journals and conferences.



**Minakshi Banerjee** received her B.Tech. (1987) and M.Tech. (1990) in Radio Physics and Electronics from the University of Calcutta and has done her Doctoral research (2008) from Jadvaypur University, Kolkata for which research work was carried out as a Senior Research Fellow (CSIR) at Indian Statistical Institute (ISI), Kolkata, India. In 1992, she joined as a Technical Officer in Government of India and worked up to 1993. She got Women Scientist Fellowship from Department of Science and Technology (DST) at Indian Statistical Institute (ISI), Kolkata, India. Presently she is a Professor, Department of Computer Science & Engineering at RCC Institute of Information Technology, Kolkata, India. Her current research interests include image processing, content-based image retrieval and soft computing.



**Rituparna Chaki** obtained her B.Tech. and M.Tech. in the department of Computer Science & Engineering from the University of Calcutta and PhD. from Jadavpur University. Presently she is a Professor of Information Technology in the A.K.Choudhury School of Information Technology at the University of Calcutta, Kolkata, India. She has published more than eighty research papers in referred journals and conferences. She is the author of several books and has edited several volumes of Springer LNCS and AISC. Her areas of research interests include Wireless Network, Cloud Computing, Ambient Intelligence, Data mining, and Image Processing.



**Punit Sharma** is presently Consultant Nuclear Medicine and PET/CT, Apollo Gleneagles Hospital, Kolkata, India. He received his MBBS degree from Calcutta Medical College, Kolkata (2000-2006), MD (Nuclear Medicine) (2007-2010) from All India Institute Of Medical Sciences (AIIMS), New Delhi, FEBNM from Vienna, Austria (2016) and FANMB from Osaka, Japan (2014). He got Asian Young Investigator Award, 2014, Japanese Society of Nuclear Medicine and SNMMI Young Professionals Committee award, 2013, SNMMI USA. He has 9 years' experience Nuclear Medicine.